ORNL/TM-2020/1606

Critical and Subcritical Californium Source Driven Noise Analysis Experiments with Fresh PWR Fuel Pins

John T. Mihalczo

March 2021

Approved for public release.
Distribution is unlimited.

ORNL/TM-2020/1606

Isotope and Fuel Cycle Technology Division

CRITICAL AND SUBCRITICAL CALIFORNIUM SOURCE DRIVEN NOISE ANALYSIS EXPERIMENTS WITH FRESH PWR FUEL PINS

John T. Mihalczo

March 2021

Prepared by
OAK RIDGE NATIONAL LABORATORY
Oak Ridge, TN 37831-6283
managed by
UT-BATTELLE, LLC
for the
US DEPARTMENT OF ENERGY
under contract DE-AC05-00OR22725

CONTENTS

LIST OF FIGURES

LIST OF TABLES

ACRONYMS

APSD	auto power spectral density
BFNA	break frequency noise analysis
CSDNA	californium source-driven noise analysis
CPSD	cross power spectral density
DOE	US Department of Energy
ICSBEP	International Criticality Safety Benchmark Program
KAPL	Knolls Atomic Power Laboratory
NMIS	Nuclear Materials Identification System
ORNL	Oak Ridge National Laboratory
ppm	parts per million
PWR	pressurized water reactor

ABSTRACT

These experiments were performed from August 1 to September 16, 1983, and used 35 operational days of critical facility time at the Babcock & Wilcox critical facility in Lynchburg, Virginia. These measurements were performed to assess the capability of the californium source-driven noise analysis method to measure the subcriticality of light water reactor fresh fuel configurations. This report documents the experiments of 1983 that were not reported at that time. These measurements with 2.459 wt. % ^{235}U-enriched uranium oxide fresh fuel pins started at the delayed critical configuration of the fully assembled pressurized water reactor (PWR) core configuration with 1,511 parts per million (ppm) boron (19.8 wt. % ^{10}B) in the water. This was a cylindrical configuration of 4,961 fuel pins. After the initial measurements at delayed criticality, subcritical measurements by the californium source-driven noise analysis method were performed, in which the number of detectors and californium source locations were varied. Additional boron was added to the water moderator and reflector to reduce the neutron multiplication factor, with resulting boron concentrations of 1,561, 1,613, 1,765, 1,880, 2,104, 2,384, 2,975, 3,606, and 4,303 ppm. After completing these measurements, the increased boron concentration was returned to that at delayed critical (1,511 ppm) and the reactivity was decreased by reducing the number of fuel pins in steps to 3,713, 2,553, 1,281, 749, and 333 fuel pins and then to that (289) of a single square 17 × 17 pin array, which approximates a single PWR fuel element. For all measurements that started at delayed criticality and then reduced the neutron multiplication factor to various subcritical states, inverse kinetics rod-drop measurements at the higher reactivities were also performed, but those results are not reported here. The break frequency noise analysis data at all subcritical states were fitted to obtain the prompt neutron decay constant. Some data presented in this report are from notes and are not in the logbook. The purpose of this report is to document the experimental information for the measurements performed so that later researchers could perform the required uncertainty and calculational analyses and documentation to use these data for an International Nuclear Criticality Safety Benchmark Program (ICSBEP) or a Nuclear Energy Agency benchmark. The data from these measurements are available from the Records Management Services Department of Oak Ridge National Laboratory, and the logbook is available from ICSBEP at Idaho National Laboratory.

1. INTRODUCTION

The applicability of the californium source-driven noise analysis (CSDNA) method [1] to determine the subcriticality of large power reactors was evaluated in 1983 in a series of measurements at the critical experiment facility of the Babcock & Wilcox Company in Lynchburg, Virginia. Because of funding limitations at the time of the measurements, the results were not documented. This report, although written much later, documents some preliminary online results. These measurements with 4,961 2.459 wt. % ^{235}U-enriched uranium oxide fresh fuel pins started at the delayed critical configuration of the fully assembled pressurized water reactor (PWR) core configuration with 1,511 parts per million (ppm) boron (19.8 wt. % ^{10}B) in the water and 4,961 fuel pins. After the initial measurements at delayed criticality, the reactivity was reduced by adding boron to the water. The increased boron concentrations were 1,561, 1,613, 1,765, 1,880, 2,104, 2,386, 2,975, 3,606, and 4,303 ppm (Appendix A). As the boron in the water was increased, the neutron energy spectrum was increased because of the additional thermal neutron absorption of additional boron in the water. The neutron multiplication factor for these subcritical configurations was determined by the CSDNA) method [1]. The break frequency noise analysis (BFNA) data [2] were fitted to obtain the break frequency which, when multiplied by 2π, gives the prompt neutron decay constant. A description of the fitting is given in Appendix B. The latter method can be used to determine the subcriticality from the prompt neutron decay constant at delayed criticality and that of the subcritical state corrected for the changes in the neutron lifetime and the delayed neutron fraction. A previous example of this for another measurement is given in Appendix C, where comparison is made with the result of CSDNA measurements for the draining tank measurements [3]. After these

measurements, the boron concentration was changed back to 1,511 ppm for the delayed critical configuration, and the measurements were repeated. Then, the number of fuel pins was reduced in steps maintaining cylindrical configurations to 3,713, 2,553, 1,281, 749, and 333. Then, a 17 × 17 fuel pin array was assembled to simulate a single fuel element, and the measurements were repeated.

The purpose of this report is to document the experimental information for the measurements performed so that later researchers could perform the required uncertainty and calculational analyses and documentation to use these data for an International Nuclear Criticality Safety Benchmark Program (ICSBEP) or a Nuclear Energy Agency benchmark. The data from these measurements are available from the Records Management Services Department of Oak Ridge National Laboratory (ORNL), and the ORNL logbook is available from ICSBEP at Idaho National Laboratory.

2. DESCRIPTION OF MATERIALS

The delayed critical configuration consisted of 4,961 fuel pins with special dry reentrant tubes for inserting the californium source and the detectors. The source locations could accommodate a one-in. -diameter californium source-ionization chamber along a diameter and at different heights. The reentrant tubes for the detectors could accommodate ½ in. diameter ^{3}He proportional counters that were 30 in. long and centrally located vertically. The fuel pins and the B_4C burnable poison pins were held in position by upper and lower grid plates in a water tank.

2.1 DESCRIPTION OF THE PINS AND WATER TANK

The sketch of a fuel pin is given in Figure 2.1, and its description is given in Table 2.1.

The location of the fuel pins and the burnable poison pins in the grid plate is depicted in Figure 2.2. The description of the fuel pins is given in Table 2.1, and a description of the B_4C pins is given in Table 2.2.

The configuration of the water tank is shown in Figure 2.3. For all but the delayed critical configuration, the water height for the core tank was 156.6 cm and that for delayed critical configuration of 4,961 fuel pins was 145 cm.

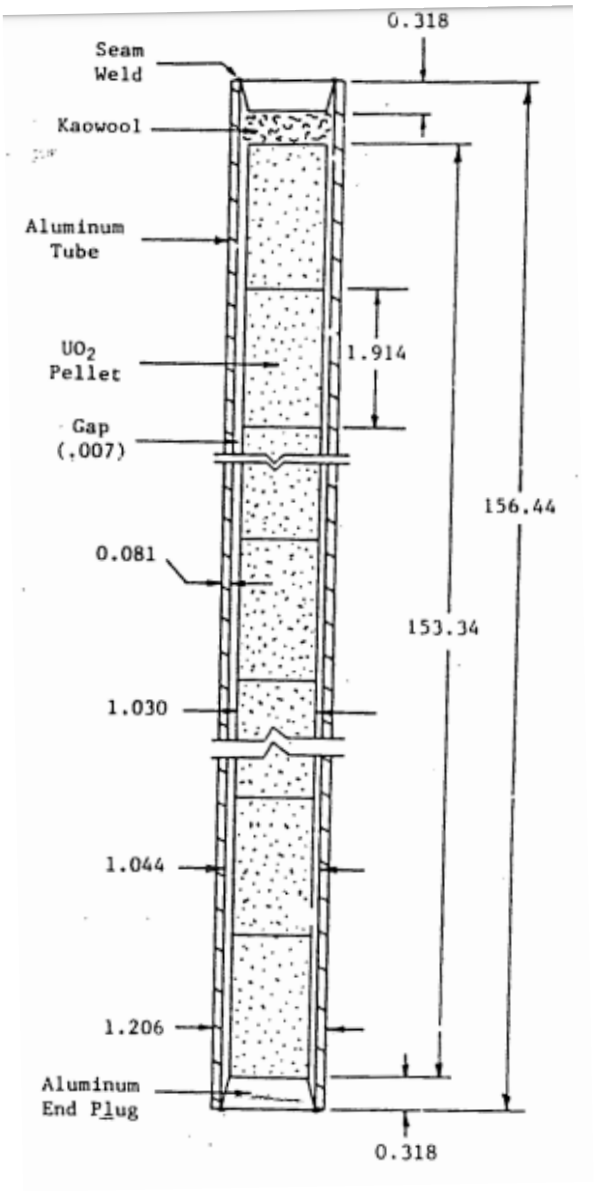

Figure 2.1. Configuration of the fuel pins.

Table 2.1. Properties of the UO_2 fuel rods (2.459 wt. % ^{235}U).

Property	Average	Standard deviation	Standard deviation of the mean
Outside diameter, cm	1.206	0.002	0.0003
Wall thickness, cm	0.081	Not given	0.003
Wall material	6061-T6 Al	Not applicable	Not applicable
Pellet diameter, cm	1.030	0.001	0.0005
Total length, cm	156.44	0.41	0.05
Active fuel length, cm	153.34	0.88	0.02
Pellet length, cm	1.914	0.008	0.002
Wt. of UO_2, g/rod	1,305.5	39.2	1.0
Wt. of U/wt. UO_2, %	88.13	0.01	0.00
Wt. of U/rod, g/rod	1,150.3	35.0	0.9
Wt. of ^{235}U, g/rod	28.29	0.86	0.02
Enrichment, wt. % ^{235}U	2.459	0.002	0.001
Pellet density, g/cm^3	10.29	0.05	0.02
Bulk density, g/cm^3	10.22	0.36	0.01
Summation of impurities, sum of $N\sigma$, cm^2/cm^3	$<4 \times 10^{-4}$	Not given	Not given

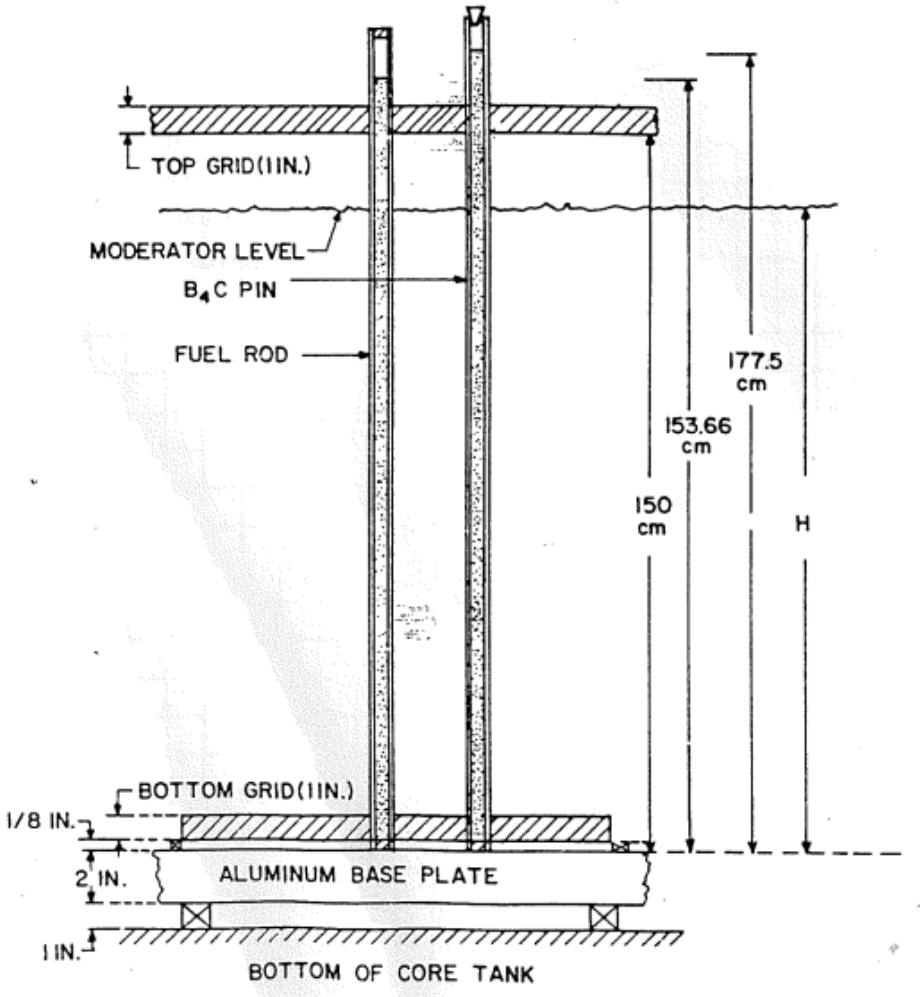

Figure 2.2. Configuration of pins in the top and bottom grid plates.

Table 2.2. Chemical analysis of the B_4C burnup pins.

Quantity	Percentage
Total boron	77.8 wt. %
Total carbon	20.8 wt. %
Anhydrous B_2O_3	0.10 wt. %
Boron plus carbon	98.6 wt. %
Particle size, 30–50 mesh	92.2 wt. %

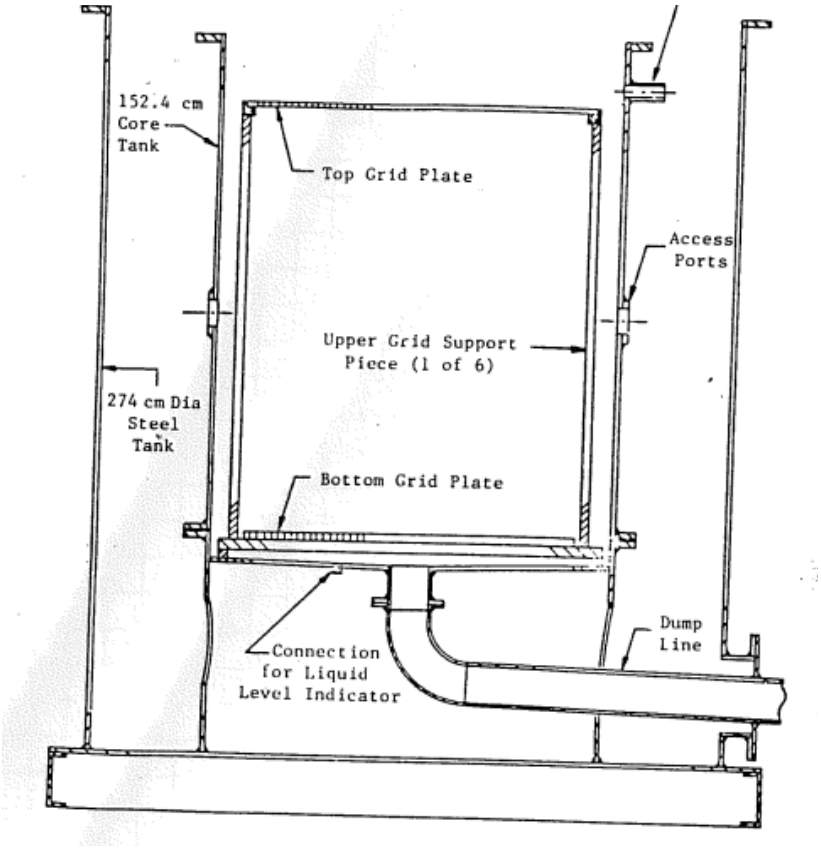

Figure 2.3. Configuration of water tank.

2.2 DESCRIPTION OF THE CALIFORNIUM SOURCE

The californium source was electroplated onto one plate of a parallel plate ionization chamber, and a sketch is shown in Figure 2.4. Using a source in an ionization chamber allowed the time tagging of the emission of neutrons from the source, which is essential for the CSDNA method. The configuration of the ionization chamber is shown in Figure 2.4, and a more detailed sketch for use in calculations can be obtained from Blakeman and Valentine's work, SUB-HEU-SOL-THERM-001[4]. The typical composition of the source is given in Table 2.3. Three sources were used in the source-driven noise measurements: 19, 21, and 22. The fission rate in source 19 was about 523,000 per second and was used in the pulse mode. Sources 21 and 22 were both at a factor of about 12 and 14 higher; they were used in the current mode where individual pulses are not detected, but the fluctuations in the current were measured. Number 19 was used at subcriticality close to delayed criticality, or somewhat below criticality. Sources 21, 22, or a combination of both were used at further subcritical where the count rates from source 19 were low. In some measurements at higher neutron multiplication factors, the higher sources were used for comparison. These comparisons allow determining the parameters required to infer the neutron multiplication factor related to using californium sources 21 and 22 in the current mode. These parameters are related to the contribution of the alpha particle events (30 times more numerous than the fission events) to the current. At the time of fabrication on July 18, 1983, these sources contained 12.09 and 13.86 μg, respectively, of ^{252}Cf, with spontaneous fission rates of more than 7 million fissions per second, which is too high for individual pulse counting. The sources were in a variety of locations in the E–W direction and vertically in the center and the outer edge of the fuel pins in the reflector. The sources were located ~0.5 cm below midplane. Most measurements were performed with the source in the center of the core where point kinetics interpretation of the ratio of spectral densities was used to infer the

neutron multiplication factor, k_{eff}. Other locations such as the top of the core and at the radial surface of the core in the reflector were used. In a few cases, two sources were used.

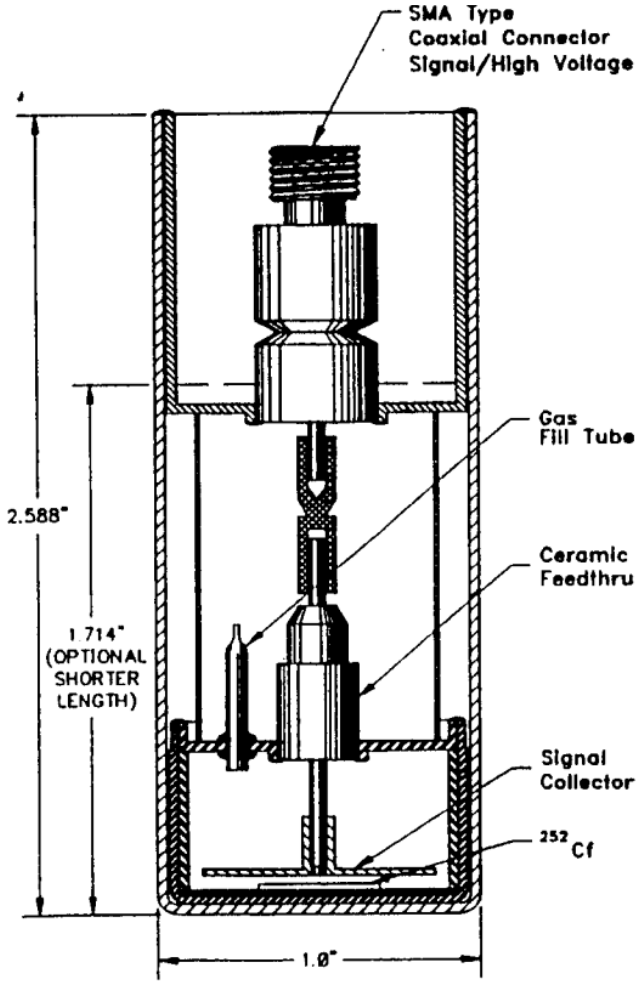

Figure 2.4 Configuration of the doubly contained stainless steel ionization chamber (1 cm diameter californium deposit).

The isotopic composition of the californium for these ionization chambers is given in Table 2.3. The composition is such that 98.8% of the neutrons are from the spontaneous fission of ^{252}Cf. Fission from other isotopes is also time tagged and included in the time-tagged californium fission rate.

Table 2.3. Composition of the californium in sources 21 and 22[a] on July 13, 1983.

Isotope	Wt. %
249	17.44
250	7.56
251	2.17
252	72.82
253	0.008
254	0.005

The source could be located at radial location along a diameter across the core but was mainly used in the center. The 2.86 cm outside diameter, 2.76-cm-inside-diameter aluminum source tubes located in the center and outer edge of the core in the reflector can be seen in Figure 2.5.

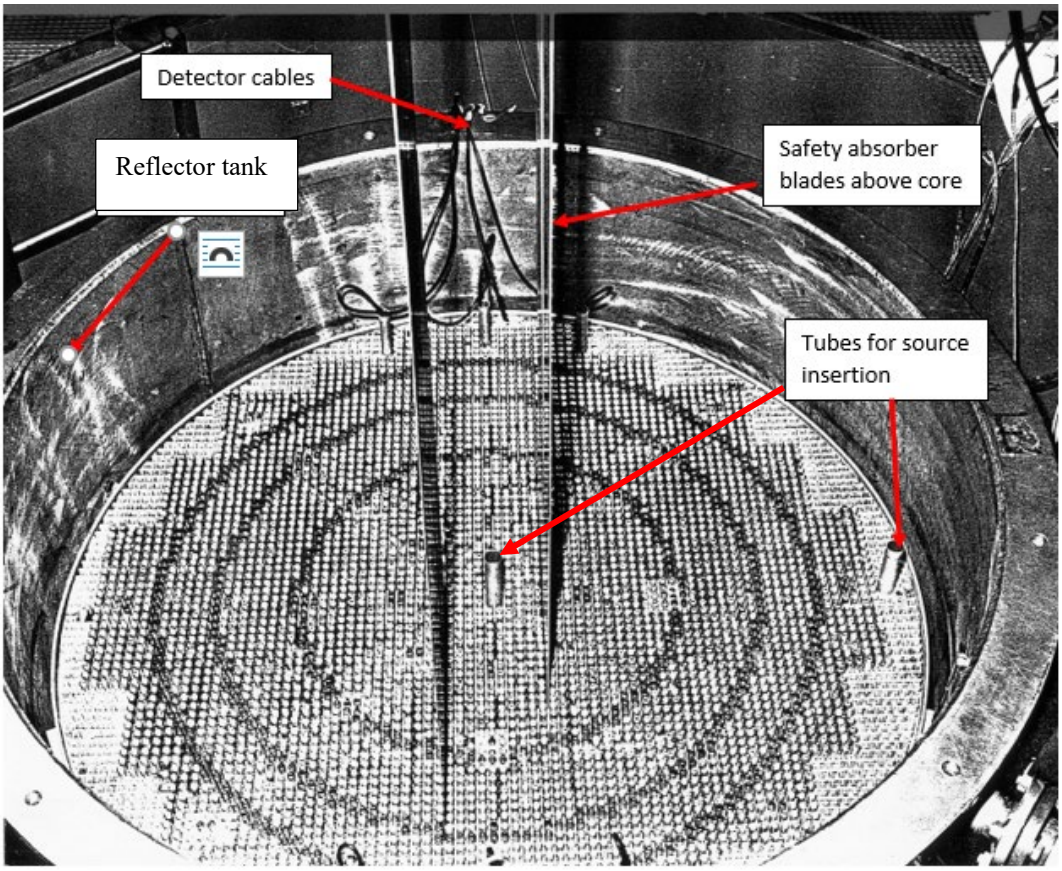

Figure 2.5. Configuration of the assembly for delayed criticality. (Larger circles in the center and the outer edge of the core on the E are source possible locations along an E–W diameter. Small circles are possible detector locations along N–S, SW–NE, and SE–NW diameters.)

The source tube in the reflector was present for most measurements with the source in the central source tube. Four fuel pins had to be removed from the array to accommodate the source tube. Only the source dry tubes in use were inserted. In a few measurements, the signals from two sources were summed and used for the source input channel. Mattingly's higher-order statistics development [5] allowed the quantitative determination of the fraction of californium fission counted in these types of chambers operated in the pulse mode and showed that 4% of the fissions were not counted. The ratio of spectral densities determined online for pulse mode data must be increased by this correction to get the true values of the measured ratio of spectral densities from what is presented in this document. The ratios of spectral densities presented in this report were obtained online at the time of the measurements, at which time the ability to determine the fraction of californium fission not counted was not available.

2.3 DESCRIPTION OF THE DETECTORS

The neutron detectors were 1.905-cm–outside diameter, 76.2-cm-long ^{3}He proportional counters (Reuter-Stokes Model # RS-P4-0630-101), and they could be in reentrant aluminum dry tubes at various locations

along diameters N–S, E–W, NW–SE, and NE–SW (Figure 2.5). To locate the detectors in the array, two fuel pins had to be removed at each detector location to insert the aluminum dry tubes that had a 2.22-cm outside diameter and a 2.13-cm inside diameter. Only detector dry tubes in use were inserted.

The data processing system had only three channels of input—one for the source and two for the detectors. In many measurements, the signals for up to three detectors were summed and used for a single detector channel input. Most experiments had six ORNL proportional counters in the system in two sets of three. The N set consisted of one detector (#6) on the N–S diameter, the second detector (#7) in the NW quadrant on the NW–SE diameter, and the third (#5) in the NE quadrant on the NE–SW diameter. The S set consisted of one detector (#2) on the N–S diameter, the second (#1) in the SE quadrant on the NW–SE diameter, and the third (#3) in the SW quadrant) on the NE–SW diameter. In most measurements, all six detectors were in the core, centered about the midplane with the water height of 156.6 cm. In some of the measurements, only one or two detectors of each set of three were used as input to the Fourier analyzer. The detectors were usually loaded at nearly the same radius. Set 1 detectors were located symmetrically to those in set 2. Two Babcock & Wilcox detectors (#4 and #8) were in the reflector adjacent to the core boundary on the N–S diameter. In some measurements at high boron concentrations, the Babcock & Wilcox detectors were included in the detector sets for the CSDNA measurements (#4 with the S set and #8 with the N set). For a few measurements, two 15.24 cm diameter scintillators were located outside and adjacent to the water reflector tank at the N and S locations. Because the detectors were located at different radii, their neutron absorption properties could change the reactivity of the configuration slightly. Detectors closer to the center would decrease the reactivity more. In any final evaluation, these effects need to be examined.

3. MEASUREMENTS AT DELAYED CRITICALITY

The first experiments performed were at delayed criticality with 4,961 fuel pins, a boron concentration of 1,511 ppm, and a water height in the core of 145 cm. After subsequent measurements with increased boron concentration, the boron concentration was returned to that for the initial criticality and the measurements repeated. The repeated boron concentration also was 1,511 ppm. The configuration of the assembly for delayed criticality is shown in Figure 3.1. If the top of the figure is designated as “N,” then the diameter E to W is where the californium source could be located in reentrant internally dry aluminum tubes. For the delayed critical configuration, the californium source was not present. The ^{3}He proportional counter could be located along diameter N–S, E–W, SW–NE, and SE–NW. The reentrant tubes for the proportional counters replaced one fuel pin location. The assembly was equipped with two neutron-absorbing safety blades for rapid shutdown of the assembly. They were inserted between two adjacent rows of fuel pins in the N–S direction. In this photograph, the safety blades were withdrawn upward. In almost all measurements, the safety blades were removed upward out of the fuel pin array. The standard configuration for this critical experiment without the reentrant tubes for the location of the source and detectors was 4,901 fuel pins. However, because of the insertion of reentrant tubes throughout the core that replaced fuel pins in the interior, 61 additional pins had to be added to achieve delayed criticality. A list of all the experimental runs for all measurements is given in Appendix D.

A cross-sectional sketch of the configuration is given in Figure 3.1 where the source and detector reentrant aluminum tube locations are specified more clearly.

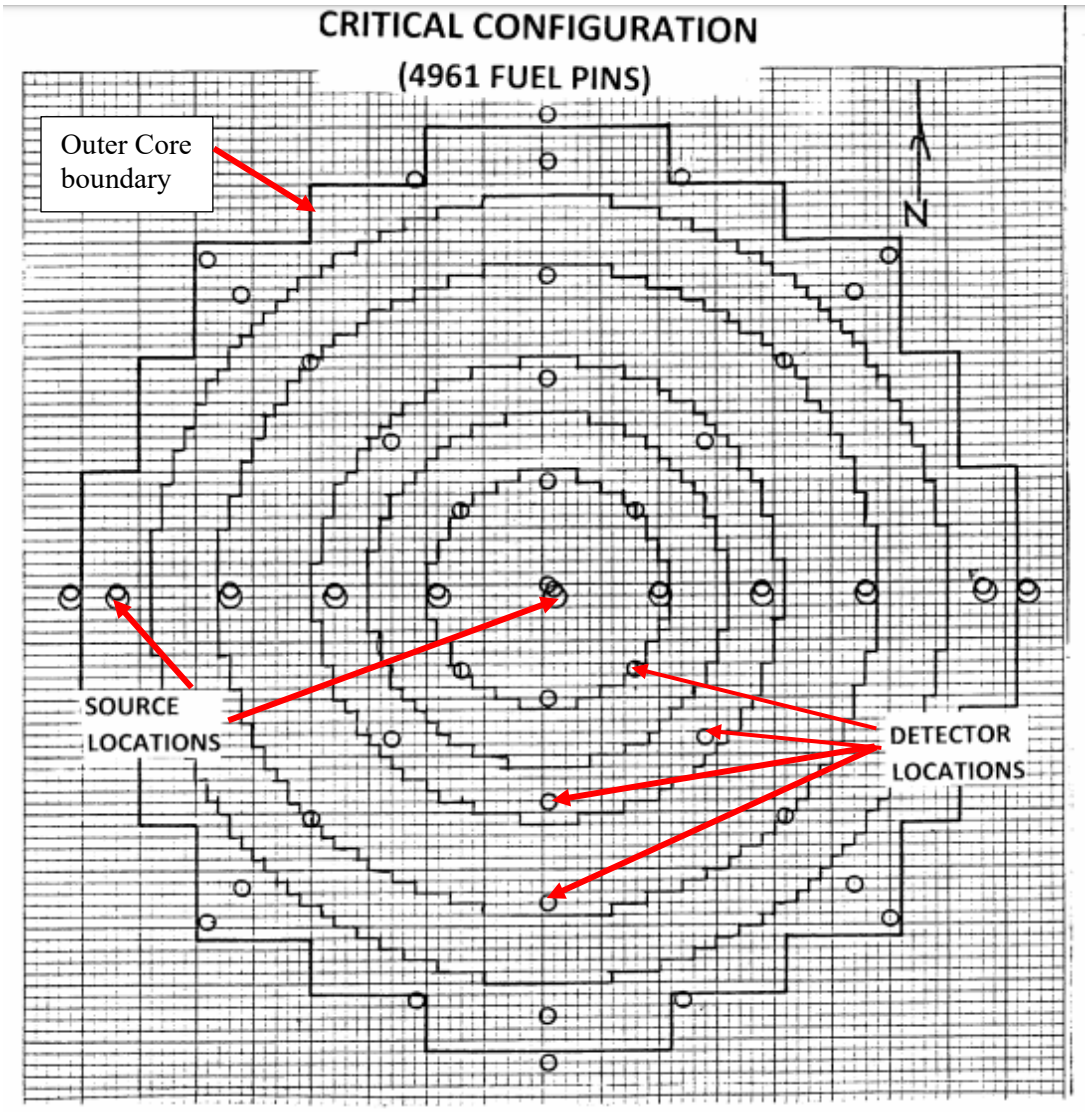

Figure 3.1. Cross section sketch of the core configuration at the vertical midplane (large circles are possible source locations; small circles are possible detector locations).

3.1 BREAK FREQUENCY NOISE ANALYSIS (BFNA)

The BFNA technique [2] determines the prompt neutron decay constant from the cross power spectral density (CPSD) between two detectors. The CPSD is the Fourier transform of the time distribution of counts (two detector Rossi-α measurement) in one detector with respect to a previous count in another detector. The break frequency is defined, and some data for these measurements are given in Appendix B. At delayed criticality, the prompt neutron decay constant is the effective delayed neutron fraction (β_{eff}) divided by the prompt neutron lifetime (l). This quantity is essential to determine the subcriticality at reduced reactivity states using the BFNA method. Four measurements were performed of the break frequency at delayed criticality: at 43.6, 43.7, 43.8, and 42.6 s^{-1}, with an average value of 43.72 ± 0.58 s^{-1}. The prompt neutron decay constant is 2π times the break frequency, or 274.7 ± 3.6 s^{-1}. With a β_{eff} value of 0.007488, the prompt neutron lifetime at delayed criticality is 0.27259 ± 0.00357 × 10^{-4} seconds, or about 27.26 μs. Some limited measurements were performed slightly below delayed critical with the critical configuration but with a water height of 145 cm. The BFNA measurements obtained prompt

neutron decay constants from the break frequencies of 50.9, 50.2, 50.2, and 52.4, which gives an average value of 50.68 ± 1.04 s^{-1} and thus a reactivity of 15.9 cents subcritical.

4. MEASUREMENTS WITH INCREASED BORON CONCENTRATION

After the repeated measurements at or near delayed criticality, the water height was returned to 156.60 cm, the boron concentration was increased in steps, and the CSDNA measurements were performed. From these measurements, the break frequency could be obtained and the subcriticality could be obtained in dollars (one dollar equals a change in k_{eff} of β_{eff}). This subcriticality in dollars, when multiplied by $\beta_{eff,}$ gives the subcriticality in units of k_{eff}. This analysis has not been performed for these measurements. The CSDNA measurement also can be used to obtain the value of k_{eff}; thus, both values could be compared. Experience has shown that the CSDNA with the ORNL interpretation of the noise equivalent source gives values of k_{eff} that agree with calculations at low values of k_{eff} (Appendix E), whereas the BFNA method usually gives good agreement only down to k_{eff} values of ~0.80. The limited interpretations of the data given in this report were performed at the time of the measurements and need further review.

4.1 CALIFORNIUM SOURCE-DRIVEN NOISE ANALYSIS

At delayed criticality, this method results in a ratio of spectral densities that is zero. However, at subcritical states, it can be measured and the subcriticality can be obtained from it. The method depends on known constants from other measurements and ratios of other quantities that can be measured or calculated. In general, ratios of quantities can be calculated more accurately than absolute values. These measurements depend on the validity of the point kinetics model for obtaining the value of k_{eff}, and many source detector locations were used where the point kinetics model was known not be valid. In general, experience has shown that the point kinetics model has validity with the source in the center and the detectors located symmetrically some distance from it.

Two formulations can be used to determine the neutron multiplication factor from the ratio of spectral densities—the Mihalczo–Paré [1] and the Akcasu–Stolle [6]. The latter is the more theoretically correct formulation. The differences are related to how the detection of the first neutron in a coincidence affects the detection of the second neutron. Other interpretations of subcritical CSDNA measurements have shown that the Akcasu–Stolle formulation gives k_{eff} values at low (<0.80) neutron multiplication factor configurations that do not agree with calculations, whereas the Mihalczo–Paré formulation gives values that agree with calculation in one case down to k_{eff} = 0.30, as shown in Appendix E. The results of two measurements that illustrate the differences in interpretation are given in Appendix E, one of which was independently analyzed by researchers at Knolls Atomic Power Laboratory and their analysis is also presented in Appendix E.

The ratio of spectral densities $R = G_{12}{}^{*}G_{13}/G_{11}G_{23}$, where G_{12} is the CPSD between detector channel 2 (can be the sum of several detector signals) and the californium spontaneous fission detection system (designated as 1), and * means the complex conjugate. G_{13} is the CPSD between detector channel 3 and the californium source. G_{11} is the auto power spectral density of the spontaneous fission detection system. G_{23} is the CPSD between detector channel 2 and detector channel 3. This ratio of spectral densities is constant at low frequency. This ratio is independent of detection efficiency by design because the detection efficiencies in the numerator are canceled by the detection efficiencies in the denominator. Thus, this ratio avoids the problem of detection efficiency by changing as the fissile system changes. These spectral densities are just Fourier transforms of the time correlation functions. The time correlation function associated with G_{23} is the time distribution of counts in detector 3 after a count in detector 2 (like two-detector Rossi-α measurement), and G_{nn} is the distribution of counts in detector n after a previous count in the same detector n (like one-detector Rossi-α measurement). The fission chains persist for a long time because water is present in the core. Because of the large number of accidental coincidences,

the fission chains overlap considerably with the californium source sizes used, which precludes measuring time correlation functions. However, measurements can be performed in the frequency domain and have been the basis of many reactor noise measurements. In fact, these types of measurements have been performed for nuclear reactors operating at 1,000 MW of power.

The data of Table 4.1 show the measured online ratios of spectral densities with their uncertainties for all subcritical measurements. These values were obtained at the time of the measurements by observing the plots of the ratio of spectral densities as a function of frequency. These values are the constant values at low frequency, and they were averaged over the region at low frequencies chosen where they were constant. For final analyses of these measurements, a more quantitative choice of the frequency range where the values are constant should be made. This is usually done varying the upper limit of the frequency range and choosing the average value with the lowest standard deviation. Where blanks or experimental runs are not listed, the data were bad or lost at the measurement site.

Table 4.1. Measured ratios of spectral densities ($\times 10^{-4}$) with uncertainties.

Run #	Ratio	Run #	Ratio	Run #	Ratio
AA	No source	AB	No source	AC	No source
AD	No source	AE	No source	AF	No source
AG	Not measured	AH	Not measured	AI	Not measured
AJ	Not measured	AK	Not measured	AL	102.6 ± 4.2
AM	109.6 ± 3.6	AN	112.6 ± 3.8	AO	9.24[a]
AP	7.4 ± 0.5	AQ	7.06 ± 0.9	AR	56.8 ± 0.9
AS	15.15 ± 0.6	AT	17.34 ± 0.98	AU	245 ± 3.8
AV	213	AW	244 ± 8.3	AX	226.7 ± 6.0
AY	35.15 ± 1.5	AZ	31.02 ± 0.95	BA	19.14 ± 1.09
BB	16.85 ± 1.1	BC	325.2 ± 7.8	BD	352.8 ± 6.2
BE	22.85 ± 1.39	BF	309.7 ± 5.1	BG	378.6 ± 10.8
BH	312.4 ± 2.3	BI	434.8 ± 5.2	BJ	475.5 ± 9.8
BK	445.9 ± 7.3	BL	938 ± 13.3	BM	988.5 ± 8.7
BN	920.0 ± 7.3	BO	817.2 ± 7.9	BP	490.4 ± 4.1
BQ	777.7 ± 9.0	BR	805.6 ± 12.8	BS	712.8 ± 11
BT	879.2 ± 20.0	BU	836.6 ± 22.5	BV	649.1 ± 8.3
BW	53.22 ± 1.9	BX	767	BY	650.2 ± 12.8
BZ	749.2 ± 12.2	CA	1,271 ± 18	CB	1,198 ± 15
CC	1,370 ± 21	CD	1,044 ± 11	CE	1,026
CF	957.3 ± 12.6	CG	1,126 ± 18	CH	1,168 ± 16
CI	757 ± 23	CJ	537.3 ± 15	CK	301
CL	910 ± 35	CM	303.8 ± 10	CN	589 ± 18
CO	110.1 ± 4.2	CP	651.8 ± 11.2	CQ	596.3 ± 13
CR	Lost or bad data	CS	820.4 ± 20	CT	Lost or bad data
CU	1,243 ± 19	CV	1,165 ± 22	CW	1,317 ± 35
CX	1,484 ± 38	CY	1,101 ± 16	CZ	1,202 ± 9
DA	929.6 ± 14	DB	962.9 ± 25	DC	729.1 ± 11
DE	849.9 ± 31	DF	1,194 ± 40	DG	206.3 ± 14
DH	206.3 ± 14	D I	138.5 ± 9.8	DJ	134.8

DK	1,835 ± 35	DL	2,886 ± 21	DM	2,654 ± 22
DN	146 ± 1.5	DO	239.1 ± 21	DP	3,540 ± 35
DQ	3,487 ± 38	DR	3,910 ± 51	DS	2,487 ± 35
DT	2,256 ± 42	DU	2,982 ± 89	DV	2,020 ± 44
DW	1,638 ± 34	DX	1,537	DY	1,537 ± 37
DZ	1,452 ± 39	EA	1,640 ± 105	EB	1,396 ± 13
EC	1,058 ± 32	ED	1,524 ± 78	EE	1,246 ± 56
EF	1,089 ± 57	EG	1,548 ± 95	EH	494.8 ± 55
EI	453 ± 29	EJ	1,158 ± 153	EK	1,300 ± 87
EL	768.4 ± 72.5	EM	140.8 ± 7.9	EN	138 ± 5.8
EO	123.8 ± 16.8	EP	119.2 ± 7.8	EQ	119.2 ± 7.8
ER	100.7 ± 6.8	ET	259.8 ± 14.3	EU	2,394 ± 59
EV	2,474 ± 92	EW	1,822 ± 56	EX	2,075 ± 159
EY	1,784 ± 51	EZ	1,385 ± 41	FA	1,918 ± 185
FB	1,948 ± 150	FC	2,234 ± 219	FE	2,060 ± 65
FF	4,385 ± 31.8	FG	4,290 ± 36	FH	4,897 ± 34
FG	4,290 ± 36	FH	4,897 ± 84	FI	2,068 ± 99
FJ	3,828 ± 156	FK	1,695 ± 34	FM	2,980 ± 216
FM	2,980 ± 216	FN	2,742 ± 231	FO	2,457 ± 35
FQ	1,295 ± 169	FR	2y,188 ± 25	FS	1,624 ± 90
FU	1,778 ± 134	FV	153.2 ± 8.7	FW	5,097 ± 285
FX	4,053 ± 97	FY	4,847 ± 57	FZ	6,291 ± 174
GA	5,943 ± 85	GB	5,358 ± 105	GC	6,525 ± 246
GD	3,803 ± 170	GE	3,349 ± 185	GG	1,791 ± 119
GH	214.5 ± 20.5	GI	349.5 ± 28	GJ	3,902 ± 6.8
GK	339.2 ± 7.1	GL	410.6 ± 8.7	GM	3,801 ± 5.5
GN	302.0 ± 7.4	GO	276.2 ± 5.9	GP	311.7 ± 4.9
GQ	287.2 ± 5	GR	259.8 ± 6.6	GS	272.2 ± 7.2
GT	Lost or bad data	GU	290.8 ± 7.3	GV	881.9 ± 9.3
GW	862.3 ± 9.9	GX	929.6 ± 17.9	GY	780.8 ± 7.5
GZ	763.8 ± 14	HA	808.2 ± 12.6	HB	712.2 ± 10.5
HC	781.3 ± 11.3	HD	643.9 ± 16.1	HE	737.4 ± 13.1
HF	1,950 ±19.8	HG	1,864 ±24.6	HH	2,101 ± 29
HI	1,795 ± 14.8	HJ	2,038 ± 19.7	HK	2,454 ± 40
HL	2,526 ± 33	HM	2,637 ± 39	HN	2,319 ± 13.5
HO	2,613 ± 19.5	HP	1,782 ± 50	HQ	1,549 ± 55
HR	2,055 ± 179	HS	1,571 ± 53	HT	2,985 ± 39
HU	2,819 ± 49	HV	3,192 ± 134	HW	3,120 ± 56
HX	2,521 ± 38	HY	3,171 ± 32	HZ	3,530 ± 45
IA	3,757 ± 50	IB	3,634 ± 46	IC	5,224 ± 53
ID	5,016 ± 49	IE	5,299 ± 115	IF	5,071 ± 88
IG	4,719 ± 54	IH	5,236 ± 62	IJ	4,111 ± 218
IK	2,987 ± 189	IL	5,409 ± 65	IM	5,598 ± 404

IN	5,072 ± 129	IO	5,436 ± 185	IP	4,925 ± 76
IQ	5,930 ± 98	IR	4,252 ± 183	IS	2,961 ± 127

[a]When uncertainties are not given they were not recorded at the time of the measurements.

The measurements with the best applicability for point kinetics and those with the best statistical precision are measurements with the N–S detector sets at the outer edge of the fissile configuration and the source in the center. By correlating the N set with the S set (on opposite sides of the core), this location ensures that most of the correlations between the two detection channels are from large fission chains that are distributed throughout the core. A small percentage of the fission chains have more than 1,000 fission (much higher than neutron multiplication would indicate), and these contribute significant coincidences to the correlation function between detection channels. Most of the correlations are from different branches in the same fission chain rather than from the same fission or the same branch of the fission chain.

To benchmark calculations, the ratios of spectral densities can be calculated directly by Monte Carlo neutron transport methods [7]. Most of these ratios were interpreted with a point kinetics model to infer the k_{eff} value, even though point kinetics is known not to be valid for some of these source–detector locations. Measured quantities will have lower uncertainty because inferred quantities have larger uncertainties because additional parameters required for interpretation of the measured data have uncertainty.

4.2 NEUTRON COUNT RATES

The neutron count rates in the detectors for all subcritical measurements are given in Appendix F. These count rates can be calculated directly with a variety of methods with the known californium fission rate. These count rates could be interpreted by the modified source multiplication method [8].

4.3 MEASUREMENTS WITH 1,511 PPM BORON, 4961 FUEL PINS WITH A WATER HEIGHT OF 145 CM

With 1,511 ppm boron in the water, the system was delayed critical and CSDNA measurements were not performed. The water height was reduced to 145 cm so that the system could be slightly subcritical and CSDNA measurements were performed. For these measurements, the detectors were centrally located two different distances (~45 and 60 cm) from the source (Cf #19 in pulse mode in the center of the core configuration). The source was also located at the top of the fuel pins and at the outer radius of the core 67.9 cm to the E. The ratios of spectral densities were interpreted using the ORNL (Mihalczo–Paré) formulation of the noise equivalent source, and the inferred neutron multiplication factors are shown in Table 4.2. Some multiplication factors are also given in parentheses for the Akcasu–Stolle formulation. Since the more theoretically correct Akcasu–Stolle theory was formulated, ORNL used both formulations for interpretation. The interpretation of the Akcasu–Stolle results suggested that, while considered to be the more theoretically correct theory, it should be improved to give the correct answers at neutron multiplication factors below $k_{eff} = 0.85$. No improvements in the theory have been made, and therefore ORNL has chosen to interpret the ratios of spectral densities using both formulations.

The uncertainty in the inferred k_{eff} values are only those associated with the uncertainty in the measured ratios of spectral densities and do not include the uncertainty in the parameters needed to obtain the k_{eff} values. The required parameters to obtain the neutron multiplication factors were from other measurements and calculations and are given in Appendix G. The required values presented in the tables for source detector locations where point kinetics were not applicable are also included in Appendix G. Usually, the model applies for central source locations with detectors symmetrically located some

distance from the source. Where the data (cross and auto power spectral densities—Fourier transforms of the auto and cross-correlation functions) were least squared fitted to obtain the break frequency, the resulting values are included in the table. The point kinetics model used to interpret the ratios is usually applicable for the central source with the detectors symmetrically located in the core centered at the midplane and far from the source. The coincidences in the detectors at large distances are preferentially from large fission chains distributed throughout the core and not from the same fission. Interpretations for source and detector locations where point kinetics are not applicable are also included. The fitted break frequencies given in Table 4.2 were essentially the same for all measurements.

Table 4.2. Neutron multiplication factors from ratios of spectral densities for 1,511 ppm boron, 4,961 fuel pins, and fitted break frequency with a water height of 145 cm.

Run identification	Neutron multiplication factor (k_{eff})	Break frequency (s^{-1})
AL	0.99791 ± 0.00009	70.2 ± 2.0
AM	0.99776 ± 0.00008	70.9 ± 1.8
AN	0.99770 ± 0.00009	70.5 ± 1.9
AO	0.99906 ± 0.000016	69.3 ± 2.4
AP[a]	0.99925 ± 0.000052	69.4 ± 2.1
AQ[a]	0.99928 ± 0.000092	69.7 ± 2.5
AR[b]	0.99599 ± 0.00011	69.4 ±1.9
AS[b]	0.99880 ± 0.000056	69.3 ±1.3
AT[b]	0.99862 ± 0.00008	69.3 ± 1.6
Average	0.99779 ± 0.00011[c]	69.78 ± 0.64[d]

[a]For runs AP and AQ the source was located at the radial surface of the core to the East.
[b]For runs AR, AS, and AT, the source was in the central source tube but at the top of the fuel pin.
[c]Runs AL, AM, and AN were used to obtain the average k_{eff} value for the configuration with the californium source in the center and the detectors symmetrically located on the N–S diameter. The average of all measurements is 0.998136 ± 0.000105.
[d]Average of all values.

At this subcriticality, using the alternate form of the noise equivalent source in the point kinetics model yields the same k_{eff} values and usually does down to k_{eff} values of 0.85.

After the measurements in Table 4.2, the boron concentration was increased to 1,561 ppm, and water height was increased to 156.6 cm.

4.4 MEASUREMENTS WITH 1,561 PPM BORON, 4,691 FUEL PINS AND A WATER HEIGHT OF 156.6 CM.

A variety of measurements were performed and the k_{eff} values determined from the ratios of spectral densities given in Table 4.1, with the ORNL point kinetics model for interpretation shown in Table 4.3. Measurements were performed with a central californium source #19 in the pulse mode with the detectors at ~30, 45, and 60 cm. Measurements were also performed with the source located at the top of the fuel pins and at the outer radius of the core. All fitted break frequencies are essentially the same. Some values for this alternate interpretation will be presented in later sections of this report at lower neutron multiplication factors. The ORNL formulation interpretation consistently gives neutron multiplication factors that agree with the calculation for a wide variety of measurements (Appendix E).

Table 4.3. Neutron multiplication factors from ratios of spectral densities for 4,961 fuel pins and 1,561 ppm boron with a water height of 156.6 cm.

Run identification	Neutron multiplication factor (k_{eff})	Break frequency (s^{-1})
AU	0.99618 ± 0.00018	98.9 ± 0.6
AV	0.99663 ± 0.00013	101.5 ± 0.6
AW	0.99388 ± 0.00024	98.5 ± 0.9
AX	0.99432 ± 0.00019	99.3 ± 0.8
AY	0.99618 ± 0.00018	100.6 ± 1.0
AZ	0.99663 ± 0.00013	98.8 ± 0.9
BA	NA[a]	100.2 ± 1.5
BB	NA	98.7 ± 1.3
Average AU-AX	0.99507 ± 0.00135[b]	99.562 ± 1.082[c]

[a]NA means not available because the online data were not recorded, or in some cases, were bad data. The same notation is used in subsequent tables.
[b]Average of measurements with source in center. The average of all measurements is 0.99660 ± 0.00064.
[c]Average of all measurements.

4.5 MEASUREMENTS WITH 1,613 PPM BORON, 4,961 FUEL PINS, AND A WATER HEIGHT OF 156.6 CM

Measurements were performed with the californium source 19 in the center top of the core, with the detectors at radial locations of ~30, 45, and 60 cm. One of the configurations of the source and detectors is given in Figure 4.1. This configuration has the best potential for point kinetics interpretation of the ratios of spectral densities to obtain the neutron multiplication factor. The neutron multiplication factors (k_{eff}) obtained from the ratios of spectral densities are given in Table 4.4.

Figure 4.1. Cross-section sketch at the midplane; one of the configurations of the source and detectors for measurements with changing boron concentrations. (Cf source in the center; small circles are possible detector locations on N–S, E–W, NE–SW, and NW–SE diameters.)

Table 4.4. Neutron multiplication factors from ratio of spectral densities and break frequency for 4,961 fuel pins, 1,613 ppm boron, and a water height of 156.6 cm.

Run identification	Neutron multiplication factor (k_{eff})	Break frequency (s^{-1})
BC	0.99010 ± 0.00031	138.5 ± 0.7
BD	0.98932 ± 0.00028	140.1 ± 0.6
BE	0.99677 ± 0.00019	140.8 ± 1.2
BF	0.99059 ± 0.00025	Not fitted
BG	0.99005 ± 0.00046	Not fitted
BH[a]	0.99559 ± 0.00033	Not fitted
BI	0.98663 ± 0.00030	Not fitted
BJ	0.98531 ± 0.00050	Not fitted
BK	0.99627 ± 0.00013	Not fitted
Average	0.99118 ± 0.00415	139.8 ± 1.2

[a]Source centered on top of core.

4.6 MEASUREMENTS WITH 1,765 PPM BORON, 4,961 FUEL PINS, AND A WATER HEIGHT OF 156.6 CM

Measurements were performed with californium source #19 in the center top of the fuel pins with the detectors at radial location of ~45 and 61 cm. The neutron multiplication factors (k_{eff}) obtained from the ratio of spectral densities and break frequency where fitted are given in Table 4.5.

Table 4.5. Neutron multiplication factors from ratio of spectral densities for 1,765 ppm boron, 4,961 fuel pins, and a water height of 156.6 cm.

Run identification	Neutron multiplication factor (k_{eff})	Break frequency (s^{-1})
BL	0.96009 ± 0.00102	248.2
BM	0.95774 ± 0.00096	234.1
BN	0.96093 ± 0.00086	257.0
BO	0.96563 ± 0.00077	277.5
BP[a]	0.93490 ± 0.00131	243.3
BQ	0.96742 ± 0.00076	
BR	0.96616 ± 0.00089	
BS	0.97032 ± 0.00076	
BT	0.96280 ± 0.00118	
BU	0.96475 ± 0.00124	
BV	0.97314 ± 0.00063	
BX	0.97089 ± 0/00057	
BY	0.97309 ± 0.00077	
BZ	0.96870 ± 0.00113	
Average: all but BP	0.96628 ± 0.00494	

[a]Source in central tube at the top of the fuel pins.

4.7 MEASUREMENTS WITH 1,880 PPM BORON, 4,961 FUEL PINS, AND A WATER HEIGHT OF 156.6 CM

Measurements were performed with a central californium source #19 with the detectors at ~30 and 45 cm. For this configuration, californium source #21 was also used in the current mode and a radial traverse from the center of the core to 61 cm W to the outer boundary, with the detectors 45 cm from the core center. The neutron multiplication factors (k_{eff}) obtained from the ratio of spectral densities are shown in Table 4.6.

Table 4.6. Neutron multiplication factors from ratio of spectral densities for 1,880 ppm boron, 4,961 fuel pins, and a water height of 156.6 cm.

Run identification	Neutron multiplication factor (k_{eff})
	Source #19 in pulse mode
CA	0.94098 ± 0.00158
CB	0.94477 ± 0.00141
CC	0.93575 ± 0.00150
CD	0.95259 ± 0.00113
CE	0.95478 ± 0.00114
CF	0.95689 ± 0.00106
CG	0.94845 ± 0.00141
CH[a]	0.94507 ± 0.00143
CI[a]	0.96174 ± 0.00076
	Source #21 in current mode
CJ[a]	0.96286 ± 0.00135
CL[a]	0.91526 ± 0.00186
CM[a]	0.98525 ± 0.00056
CN[a]	0.95903 ± 0.00160
CO[a]	0.98286 ± 0.00070
CP	0.96009 ± 0.00114
CQ	0.96370 ± 0.00115
CR	NA
CS	0.94857 ± 0.00176

[a]Radial source traverse.

The values using source #21 differ from those for californium source #19 probably because of the improper parameters associated with current mode operation of the ionization chamber for the source.

4.8 MEASUREMENTS WITH 2,104 PPM BORON, 4,961 FUEL PINS, AND A WATER HEIGHT OF 156.6 CM

Most of the measurements for this boron concentration were with californium source #21; a single measurement with californium source #19 was used. Two measurements at different radii were also performed with both Sources #21 and #22 simultaneously at the same two radial locations—one on the E and the other W. The current mode signals for both sources were summed and input to the source channel

in the processor. The neutron multiplication factors (k_{eff}) obtained from the ratio of spectral densities are given in Table 4.7.

Table 4.7. Neutron multiplication factors from ratio of spectral densities for 2,104 ppm boron, 4,961 fuel pins, and a water height of 156.6 cm.

Run identification	Neutron multiplication factor (k_{eff})
	Source #21
CU	0.90997 ± 0.00277
CV	0.91652 ± 0.00265
CW	0,90363 ± 0.00381
CX	0.88881 ± 0.00444
CY	0.92114 ± 0.00221
CZ	0.92040 ± 0.00353
DA	0.93547 ± 0.00177
DB	0.95263 ± 0.00165
DC	0.94697 ± 0.00138
DD	0.93261 ± 0.00292
DE	0.94162 ± 0.00267
DF	0.91410 ± 0.00389
DG	NA
DH	0.97182 ± 0.00202
DI	0.95666 ± 0.00317
	Source #22
DJ	0.99153 ± 0.00489
DK	NA
	Source #19
DL	0.82673 ± 0.00552
DM	0.76117 ± 0.00911
	Source #21 and #22
DN	0.95619 ± 0.00306
DO	0.98490 ± 0.00142

4.9 MEASUREMENTS WITH 2,386 PPM BORON, 4,961 FUEL PINS, AND A WATER HEIGHT OF 156.6 CM

Measurements were performed with source #19 in the center of the core with the detectors at radii of ~15 and 30 cm. Measurements were also performed with californium sources #21 and #22, a single-source radial traverse at the core centerline, and a two-source traverse with the two sources on top of the fuel pins. For some of these locations, clearly, point kinetics do not apply, but the interpretations of the ratio of spectral densities were performed anyway. The neutron multiplication factors (k_{eff}) obtained from the ratio of spectral densities are shown in Table 4.8.

Table 4.8. Neutron multiplication factors from ratio of spectral densities for 2,386 ppm boron, 4,961 fuel pins, and a water height of 156.6 cm.

Run identification	Neutron multiplication factor, (k_{eff})[a]
	Source #19
DP	0.75737 ± 0.00919 (0.80488)
DQ	0.76254 ± 0.00903 (0.808233)
DR	0.71941 ± 0/01300 (0.78108)
DS	0.84987 ± 0.00500 (0.85874)
DT	0.86623 ± 0.00268 (0.88203)
DU	0.80859 ± 0.00967 (0.83743)
	Source #22
DV	0.82659 ± 0.00729
DW	0.92247 ± 0.00336
	Source #21
DY	0.87708 ± 0.00477
DZ	0.88506 ± 0.00468
EA	0.86691 ± 0.01110
EB	0.89055 ± 0.00484
EC	0.92077 ± 0.00362
ED	0.87835 ± 0.00218
EE	0.90308 ±0.00564
EF	0.93159 ± 0.00508
EJ	0.91211 ± 0.01374
EG	0.87135 ±0.01015
EI	0.96136 ± 0.00272
EJ	0.91211 ± 0.13744
EK	0.89942 ± 0.00829
EL	0.94459 ± 0.00586
EM	0.99047 ± 0.00057
EN	0.99066 ±0.00627
EO	0.99035 ±0.00066
EP	0.96558 ±0.00335
EQ	0.99689 ± 0.00226
ER	0.97800 ±0.00196
ET	0.0.96298 ±0.00220

[a] Values in parentheses are obtained with the Akcasu–Stolle formulation, and the uncertainties were not recorded online.

The results for the Akcasu–Stolle formulation are a few percent higher than for the Mihalczo–Paré formulation for this configuration.

4.10 MEASUREMENTS WITH 2,925 PPM BORON, 4,961 FUEL PINS, AND A WATER HEIGHT OF 156.6 CM

Measurements were performed with californium sources #21 and #22 with the detectors at the larger radii and one measurement with californium #19 at a radius of 15 cm. For some of these measurements, the Babcock & Wilcox detectors in the reflector at the outer edge of the core were included in detector processor channels two and three. The neutron multiplication factors (k_{eff}) obtained from the ratio of spectral densities are given in Table 4.9.

Table 4.9. Neutron multiplication factors from ratio of spectral densities for 2,925 ppm boron, 4,961 fuel pins, and a water height of 156.6 cm.

Run identification	Neutron multiplication factor (k_{eff})[a]
	Source #21
EU	0.76339 ± 0.01140
EV	0.75239 ± 0.01528
EW	0.81293 ± 0.01037
EX	NA
EY*	0.83901 ± 0.00916
EZ	0.88174 ± 0.00505
FA	0.82355 ± 0.02233
FB*	0.82000 ± 0.01883
	Source #22
FC	0.80600 0.01825
FE	0.85930 ± 0.00649
FI	0.80550 ± 0.01350
	Source #19
FF	0.63533 (0.73190)
FG	0.64853 (0.7863)
FH	0.6504 (0.69476)

[a] Values in parentheses are obtained with the Akcasu–Stolle formulation, with the uncertainty not recorded online.

The values for sources #21 and #22 do not agree with those from source #19 because the values in the online interpretation associated with the current mode of operation of sources #21 and #22 are possibly not correct. The values from the Akcasu–Stolle formulation are considerably higher than from the Mihalczo–Paré formulation, which is consistent with the interpretation of the other measurements.

4.11 MEASUREMENTS WITH 3,606 PPM BORON, 4,961 FUEL PINS, AND A WATER HEIGHT OF 156.6 CM

Most of these measurements were performed with californium source #22, with a few measurements with californium source #19. The neutron multiplication factors (k_{eff}) obtained from the ratio of spectral densities are provided in Table 4.10.

Table 4.10. Neutron multiplication factors from ratio of spectral densities for 3,606 ppm boron, 4,961 fuel pins, and a water height of 156.6 cm.

Run identification	Neutron multiplication factor (k_{eff})
	Source #22
FJ	0.51810 ± 0.04524
FK	0.84563 ± 0.00562
FL	NA
FM	0.66866 ± 0.0386
FN	0.70710 ± 0.03742
FQ	0.88835 ± 0.01730
FU	0.836156 ± 0.01611
FW	NA
FX	0.43572 ± 0.04129
	Source #19
FY	0.56490 ± 0.02242
FZ	NA

4.12 MEASUREMENTS WITH 4,303 PPM BORON, 4,961 FUEL PINS, AND A WATER HEIGHT OF 156.6 CM

Measurements were performed with californium sources #22 and #19 in the center of the core. The neutron multiplication factors (k_{eff}) obtained from the ratio of spectral densities are shown in Table 4.11. The values using the Akcasu–Stolle formulation are significantly higher than with the Mihalczo–Paré formulation.

Table 4.11. Neutron multiplication factors from ratio of spectral densities for 4,303 ppm boron, 4,961 fuel pins, and a water height of 156.6 cm.

Run identification	Neutron multiplication factor (k_{eff})[a]
	Source #19
GA	0.40762 ± 0.03950 (0.62549)
GB	0.50337 ± 0.03226 (0.6664)
GC	0.32298 ± 0.09820
	Source #22
GD	0.50487 ± 0.04749
GE	0.61321 ± 0.04021

[a] Values in parentheses are obtained with the Akcasu–Stolle formulation, with uncertainties not recorded online.

5. MEASUREMENTS WITH REDUCED NUMBERS OF FUEL PINS

After the increased boron concentration measurements and repeated delayed criticality configurations, the numbers of fuel pins were reduced in cylindrical configurations in the following order: 3,713, 2,553, 1,281, 749, and 333. The water height was 156.6 cm for all these measurements. To help reduce the number, the fuel pins were marked on the top. The photograph in Figure 3.1 indicates the outline of some of the configurations. The reduced fuel pin configurations are given in Figures 5.1–5.5. The final fuel pin configuration was a 17 × 17 fuel pin array representing a single PWR fuel element, which is shown in Figure 5.6.

5.1 MEASUREMENTS WITH 3,713 FUEL PINS, 1,511 PPM BORON, AND A WATER HEIGHT OF 156.6 CM

A cross sectional sketch at the midplane of the core for this configuration is given in Figure 5.1.

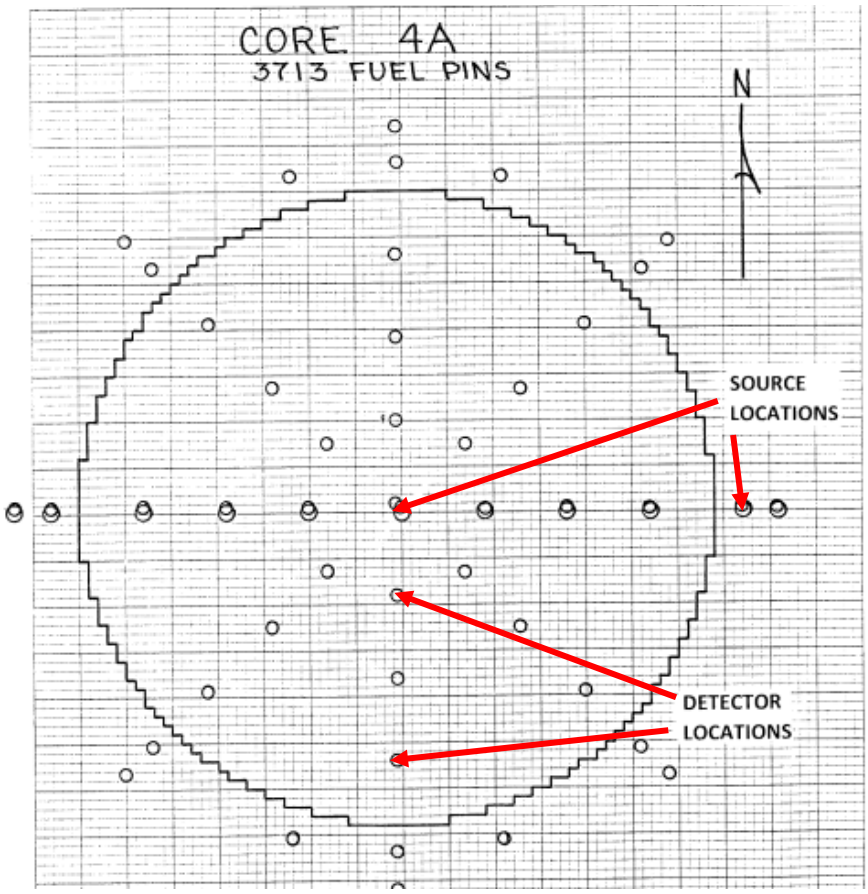

Figure 5.1. Sketch of the 3,713 fuel pin configurations (Squares are fuel pin locations; large circles are possible source locations; small circles are possible detector locations.)

Measurements were only performed with californium source #19 with the detectors at radii of ~30, 45, and 60 cm. The neutron multiplication factors (k_{eff}) obtained from the ratio of spectral densities are given in Table 5.1.

Table 5.1. Measurements with 3,713 fuel pins, 1,511 ppm boron, and a water height of 156.6 cm.

Run identification	Neutron multiplication factor (k_{eff})[a]
GJ	0.99781 ± 0.00034 (0.9881 ± 0.0030)
GK	0.98899 ± 0.00031 (0.9892 ± 0.00030)
GL	0.98658 ± 0.00039 (0.9861 ± 0.0004)
GM	0.98753 ± 0.00035 (0.9879 ± 0.00030)
GN*	0.99023 ± 0.00030 (0.9904 ± 0.0003)
GO	0.99109 ± 0.00025

Run identification	Neutron multiplication factor (k_{eff})[a]
	(0.9914 ± 0.0002)
GP	0.99031 ± 0.00026 0.9904 ± 0.0002)
GQ	0.99073 ± 0.00024 (0.9909 ± 0.0002)
GR*	0.99163 ± 0.00027 (0.0018 ± 0.0002)
GS	0.99122 ± 0.00029 (0.9914 ± 0.0002
GU	0.99088 ± 0.00034 (0.9910 ± 0.0002
Average	0.98993 ± 0.00172

[a] Values in parentheses are obtained with Akcasu–Stolle formulation.

5.2 MEASUREMENTS WITH 2,553 FUEL PINS, 1,511 PPM BORON, AND A WATER HEIGHT OF 156.6 CM

A cross-sectional sketch at the midplane of the core for this configuration is shown in Figure 5.2.

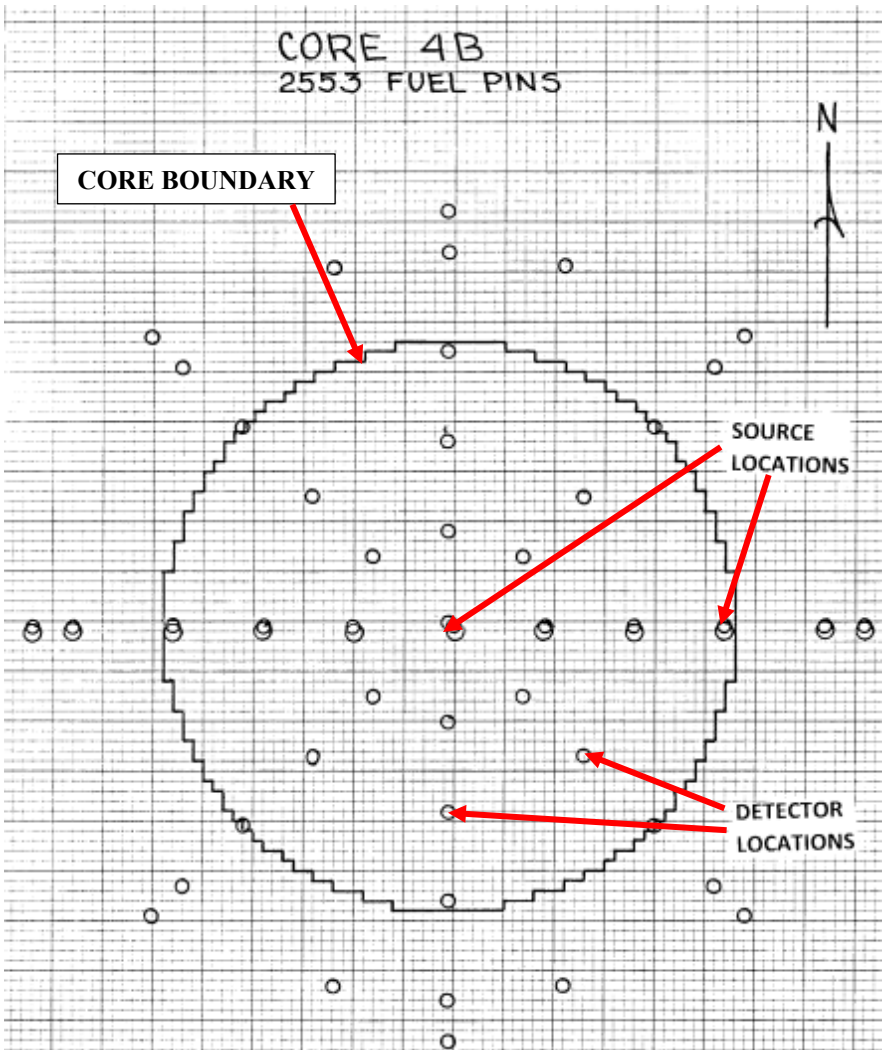

Figure 5.2. Sketch of the 2,553 fuel pin configurations. (Squares are fuel pin locations; large circles are possible source locations; small circles are possible detector locations).

Measurements were only performed with californium source #19 with the detectors at radii of ~30, 45, and 60 cm. The neutron multiplication factors (k_{eff}) obtained from the ratio of spectral densities are given in Table 5.2.

Table 5.2. Measurements with 2,553 fuel pins, 1,511ppm boron, and a water height of 156.6 cm.

Run identification	Neutron multiplication factor (k_{eff})[a]
GV*	0.96299 ± 0.00086 (0.9630 ± 0.0006)
GW	0.96388 ± 0.00085 (0.9695 ± 0.0007)
GX	0.96080 ± 0.00114 0.9627 ± 0.0009
GY*	0.96755 ± 0.00072 (0.9689 ± 0.0006)
GZ	0.96942 ± 0.00097 (0.9696 ± 0.0007
HA	0.96632 ± 0.00087)
HB*	0.97057 ± 0.00082 (0.9717 ± 0.0006)
HC	0.96753 ± 0.00082 (0.9689 ± 0.0007)
HD	0.97358 ± 0.00087 (0.9745 ± 0.0006)
HE	0.96948 ± 0.00083 (0.9767 ± 0.0007)
Average	0.96691 ± 0.0040

[a] Values in parentheses are obtained with Akcasu–Stolle formulation.

5.3 MEASUREMENTS WITH 1,281 FUEL PINS, 1,511 PPM BORON, AND A WATER HEIGHT OF 156.6 CM

A cross sectional sketch at the midplane of the core for this configuration is given in Figure 5.3.

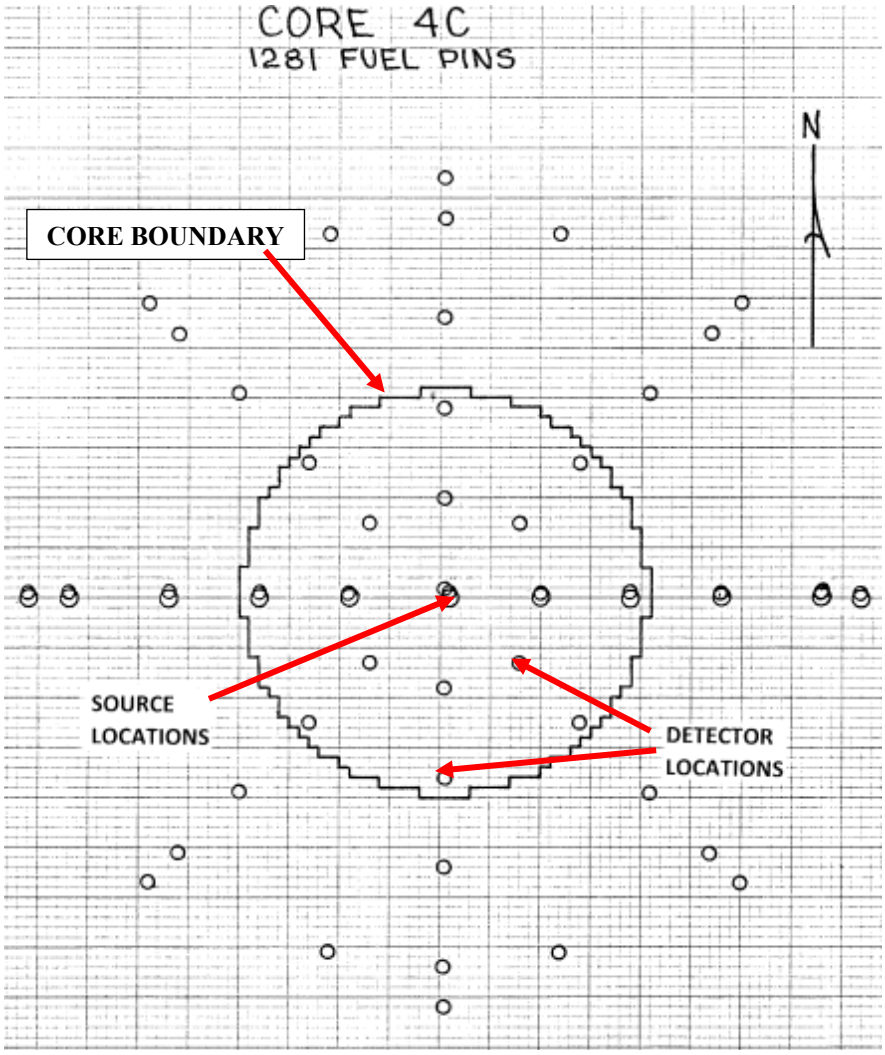

Figure 5.3. Sketch of the 1,281 fuel pin configurations. (Large circles are possible source locations; small circles are possible detector locations.)

Measurements were only performed with californium source #19 with the detectors at radii of ~15, 30, and 45 cm. The neutron multiplication factors (k_{eff}) obtained from the ratio of spectral densities are given in Table 5.3.

Table 5.3. Measurements with 1,281 fuel pins, 1,511ppm boron, and a water height of 156.6 cm.

Run identification	Neutron multiplication factor (k_{eff})
HF*	0.90642 ± 0.00260
HG	0.91137 ± 0.00260
HH	0.89750 ± 0.00316 (0.90797)
HI	0.91528 ± 0.00221
HJ	0.90309 ± 0.00289
HK*	0.87546 ± 0.00434 (0.89059)
HL	0.87073 ± 0.00426 (0.88697
HM	0.86330 ± 0.00499 (0.88133)
HN	0.88409 ± 0.00326 (0.89731)
HO	0.86492 ± 0.00412 (0.88256)
HP*	0.91601 ± 0.00346
HQ	0.92875 ± 0.00336
HR	0.90025 ± 0.01094
Average	0.89517 ± 0.02139

[a] Values in parentheses are obtained with the Akcasu–Stolle formulation. Where uncertainties were not given for the Akcasu–Stolle formulation, they were not recorded online.

5.4 MEASUREMENTS WITH 749 FUEL PINS, 1,511 PPM BORON, AND A WATER HEIGHT OF 156.6 CM

A cross-sectional sketch at the midplane of the core for this configuration is given in Figure 5.4.

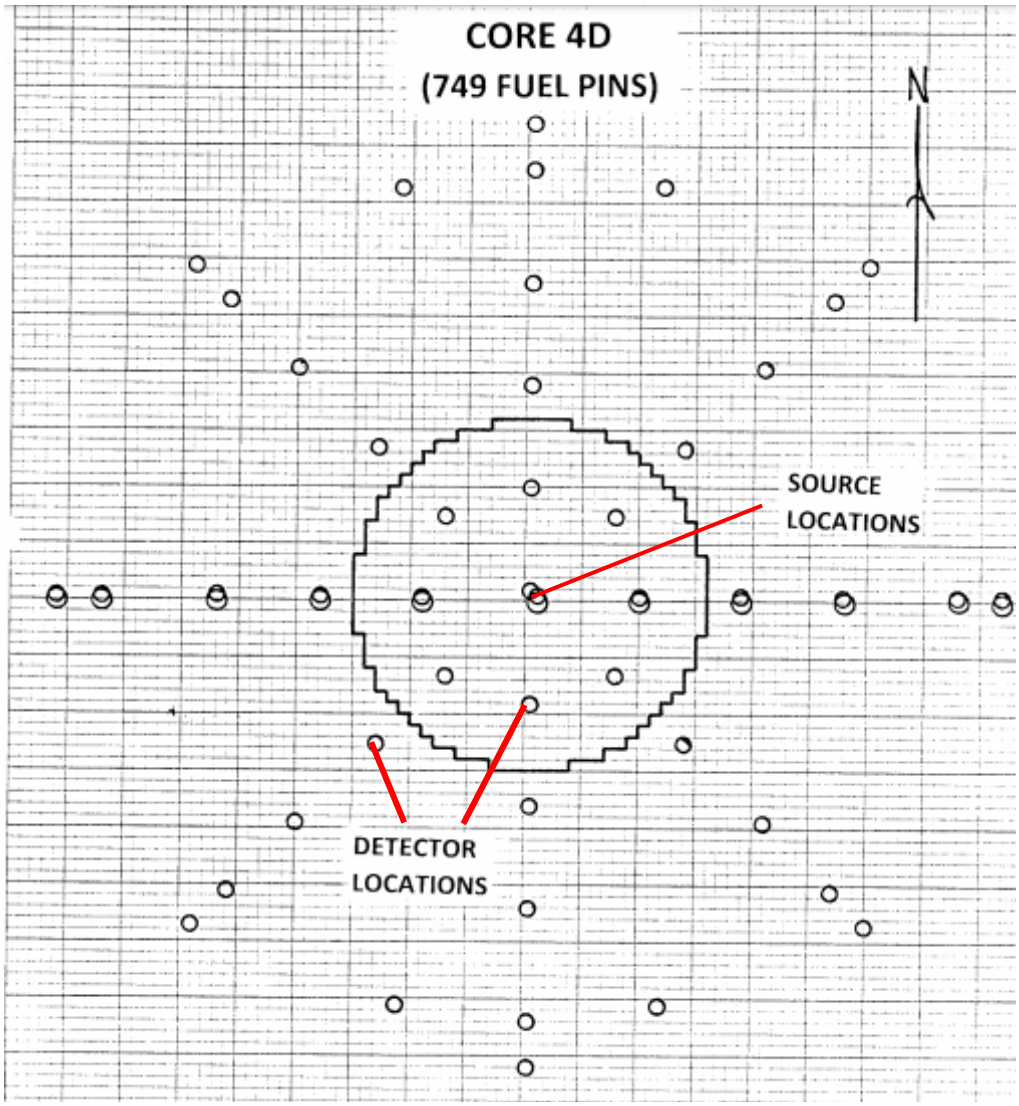

Figure 5.4. Sketch of the 749 fuel pin configurations. (Large circles are possible source locations; small circles are possible detector locations.)

Measurements were only performed with californium source #19 with the detectors at radii of ~15 and 30 cm. The neutron multiplication factors (k_{eff}) obtained from the ratio of spectral densities are given in Table 5.4.

Table 5.4. Measurements with 749 fuel pins, 1,511ppm boron, and a water height of 156.6 cm.

Run identification	Neutron multiplication factor (k_{eff})
HT*	0.8230 ± 0.0039 (0.8520 ± 0.0029
HU	0.8063 ± 0.104 (0.8405 ± 0.0072)
HV	0.8059 ± 0.0116 (0.8402 ± 0.0080
HW	0.8119 ± 0.0053 (0.8443 ± 0.0038
HX	0.8583 ± 0.0034 (0.8777 ± 0.0027
HY*	0.76301 ± 0.00923 (0.8480 ± 0.0032)
HZ	0.77618 ± 0.00897 (0.8204 ± 0.0036)
IA	0.72459 ± 0.01347 (0.8157 ± 0.0035)
IB	0.77110 ± 0.00947 (0.8177 ± 0.0039)

[a] Values in parentheses are obtained with Akcasu–Stolle formulation.

5.5 MEASUREMENTS WITH 333 FUEL PINS, 1,511 PPM BORON, AND A WATER HEIGHT OF 156.6 CM

A cross sectional sketch at the midplane of the core for this configuration is given in Figure 5.5.

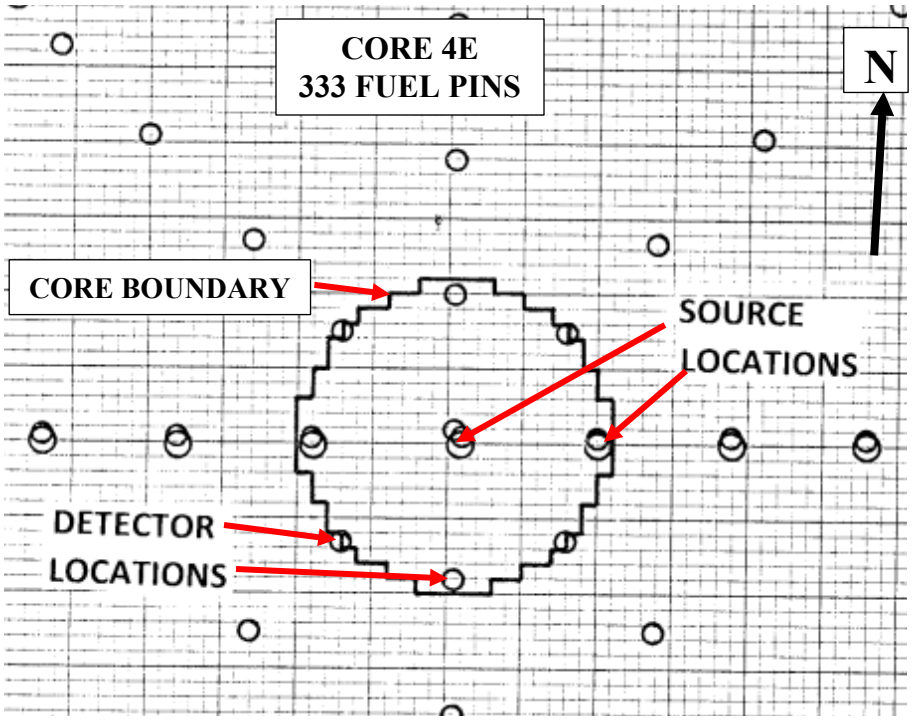

Figure 5.5. Sketch of the 333 fuel pin configurations. (Large circles are possible source locations; small circles are possible detector locations.)

Measurements were performed with californium source #19 in the center of the fuel pins, with the detectors at a radius of ~15 cm. One measurement was performed with the detectors in the borated water at a radius of ~30 cm. The neutron multiplication factors (k_{eff}) obtained from the ratio of spectral densities are given in Table 5.5.

Table 5.5. Measurements with 333 fuel pins, 1,511ppm boron, and a water height of 156.6 cm.

Run identification	Neutron multiplication factor (k_{eff})
IC	0.59745 ± 0.02387 (0.7149 ± 0.0059)
ID	0.61191 ± 0.02146 (0.7293 ± 0.0055)
IE	0.57059 ± 0.02995 (0.6983 ± 0.0122)
IF	0.60417 ± 0.02444 (0.7255 ± 0.0025)
IG	0.72825 ± 0.01268 (0.7493 ± 0.0055)
IH	0.58012 ± 0.02509 (0.7141 ± 0.0065

5.6 MEASUREMENTS WITH 289 FUEL PINS, 1,511 PPM BORON, AND A WATER HEIGHT OF 156.6 CM

CSDNA measurements were performed with californium source #19 with the detectors at the outer surface of the array and the source in the center. Measurements were also performed with the detectors far out in the reflector. In the array, detector 1 was in the SE corner, detector 2 was directly S and adjacent to the array, detector 3 was in the SW corner, detector 5 was in the NE corner, detector 6 was directly N and adjacent to the array, and detector 7 was in the NW corner in the array. A cross-sectional sketch at the midplane of the core for this configuration is given in Figure 5.6.

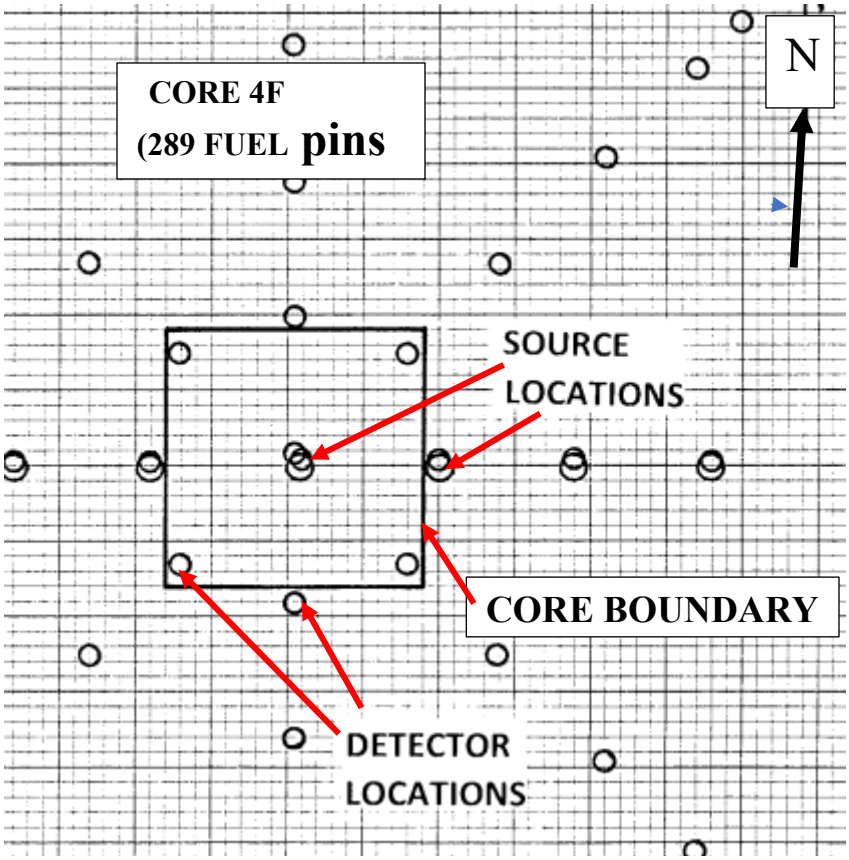

Figure 5.6. Sketch of the 289 fuel pin configurations (large circles are possible source locations; small circles are possible detector locations).

Measurements were performed with californium source #19 in the center of the configuration and with the source adjacent to the outer fuel pins centered vertically. The neutron multiplication factors (k_{eff}) obtained from the ratio of spectral densities are given in Table 5.6.

Table 5.6. Measurements with 269 fuel pins, 1,511ppm boron, and a water height of 156.6 cm.

Run identification	Neutron multiplication factor (k_{eff})
IL*	0.54715 ± 0.02822 (0.6978 ± 0.0061)
IM	0.51588 ± 0.03457 (0.6842 ± 0.0082)
IN	0.42757 ± 0.0478 (0.6485 ± 0.0110)
IO	0.53630 ± 0.04083 (0.6930 ± 0.0114
IP	0.61882 ± 0.02199 (0.7318 ± 0.0063)
IQ	0.45566 ± 0.04109 (0.0.6594 ± 0.0.0087
IR	0.7029 ± 0.210 (0.7768 ± 0.120)
IS	0.8246 ± 0.0100 (0.8536 ± 0.0071)

[a] Values in parentheses are obtained with the Akcasu–Stolle formulation and are generally larger than those from the Mihalczo–Paré formulation, especially at low neutron multiplication factors.

6. OTHER MEASUREMENTS

Inverse kinetics rod-drop measurements [9] were performed at near delayed criticality and with 4,961 fuel pins and boron concentrations up to 1,765 ppm natural boron. In these measurements, one or both safety blades were dropped into the core. Interpretation of these measurements uses the resulting decay of the neutron decay of the count rate (mostly determined by prompt and delayed neutron decay) to infer the initial reactivity.

7. CONCLUSIONS

The data presented in this report document the experimental information obtained by Oak Ridge National Laboratory (ORNL) for configurations of pressurized water reactor fresh fuel pins at the Babcock & Wilcox critical experiments facility in Lynchburg, Virginia, in 1983. The experimental data presented in this report provide several opportunities for benchmarks to be included in International Criticality Safety Benchmark Program (ICSBEP) for configurations of fresh pressurized water reactor fuel pins with 2.495 wt. % ^{235}U. A delayed critical configuration benchmark could be prepared if researchers perform the uncertainty analyses, calculations, and documentation required for ICSBEP benchmarks. A benchmark could also be performed for the measured prompt neutron decay constant for the delayed critical configuration. As natural boron (19.8 wt. % ^{10}B) was added to the water moderator, the neutron spectra shift to higher energy as the boron in the water moderator and reflector absorbs more thermal neutrons. These higher borated water configurations (from 1,511 ppm at delayed critical up to 4,303 ppm) could also be benchmarked, as well as the configurations with reduced numbers of fuel pins (from 4,961 at delayed critical down to 289 fuel pins with 1,511 ppm boron). The experimental data recorded online

need to be reevaluated. The data from the measurements are available from ORNL Records Management Services Department, and the logbook is available from John Bess at Idaho National Laboratory.

The benchmarks could be performed for directly measured quantities, such as the ratio of spectral densities, prompt neutron decay constants, count rates, or neutron multiplication factors obtained from the ratio of spectral densities. Directly measured quantities will have lower uncertainties than inferred quantities because additional parameters to interpret the measured data have uncertainties, such as the neutron multiplication factor from the Californium source driven noise analysis measurements.

ACKNOWLEDGMENTS

ORNL acknowledges the help of Dr. Neil Baldwin and the staff of the Babcock & Wilcox critical experiments facility for their cooperation in performing the measurements and providing the data that describe the experimental configurations.

REFERENCES

1. J. T. Mihalczo and V. K. Paré, "Theory of Correlation Measurement in Time and Frequency Domains with ^{252}Cf," *Ann. Nucl. Energy*, **2**, 97–105 [OSTI #4243449] (1975).
2. R. E. Uhrig, *Random Noise Techniques in Nuclear Reactor Systems*, The Ronald Press (January 1970).
3. J. T. Mihalczo, E. D. Blakeman, G. E. Ragan, E. B. Johnson, and Y. Hachiya, "Dynamic Subcriticality Measurements Using the ^{252}Cf-Source-Driven Noise Analysis Method," *Nucl. Sci. Eng.*, **104**, no. 4, 314–338 (1990).
4. T. E. Valentine and E. D. Blakeman, Unreflected High-Enriched Uranyl Nitrate Subcritical Noise, INCSBEP benchmark program at Idaho National Laboratory, SUB-HEU-SOL-THERM-001, NEA/NSC/DPC (95)03/Vol II (2019).
5. J. Mattingly, "Higher Order Statistical Signatures from Source Driven Measurements of Subcritical Systems" University of Tennessee PhD Dissertation (1998)
6. A.Z. Akcasu and A. Stolle, "Langevin Equation Approach to Reactor Noise Analysis: Stochastic Transport Equation," *Nucl. Sci. Eng.*, **113**, no. 1, 31–55 (1993).
7. S. A. Pozzi, E. Padovani, and M. Marseguerra, "MCNP-PoliMi: A Monte Carlo Code for Correlation Measurements," Nuclear Instruments and Methods in Physics Research Section A, 513/3 pp. 550-558, 2003. 116.
8. J. T. Mihalczo, A Review of Methods for Treatment of Source Effects in the Modified Source Multiplication Method for Monitoring the Reactivity in Refueling the CRBR, ORNL-5568, Union Carbide Corp. Nuclear Division, Oak Ridge National Laboratory [OSTI #5984287] (September 1979).
9. J. B. Bullock, J. T. Mihalczo, and M. V. Mathis, Inverse Kinetics Rod Drop Measurements with a Mock-Up of the Clinch River Breeder Reactor Shield, ORNL/TM-4828, Union Carbide Corp. Nuclear Division, Oak Ridge National Laboratory [OSTI #4276047] (1976).

APPENDIX A. BORON ANALYSIS OF WATER

The following table (A.1) gives the results of the natural boron analysis. The close correspondence of the desired boron concentration with the measured indicates the precise control of the boron content. The uncertainties in the measured boron concentrations are 3 ppm.

Table A.1. Results of the boron analysis.

Date Sample Was Taken	Analysis Run Number	Previously Estimated Moderator Boron Concentration (ppm)	Measured Moderator Boron Concentration (ppm)
8-1-83	2921	1510	1511
8-3-83	2923	1552	1561
8-4-83	2924	1602	1613
8-5-83	2925	1752	1765
8-9-83	2927	1860	1880
8-11-83	2929	2080	2104
8-18-83	2933	2340	2386
8-25-83	2938	2850	2925
8-30-83	2941	3500	3606
9-7-83	2947	4147	4303
9-8-83	2948	2340	2439
9-12-83	2951	1510	1510
9-14-83	2955	1510	1511

APPENDIX B. BREAK FREQUENCY NOISE ANALYSIS AND PROMPT NEUTRON DECAY CONSTANT

This appendix summarizes the break-frequency noise analysis and how it can be used to determine the subcriticality. The break frequency, sometimes is called the cutoff frequency, is the frequency at which the response initiates its decrease (Figure B.1). This frequency is determined by fitting the cross or auto spectral densities to an amplitude and a break frequency. The data can be fitted to one break frequency because the point kinetics model is applicable, which is usually true for neutron multiplication factors above 0.80. At further subcritical, this model does not work because the data cannot be fitted in this manner to a single break frequency. This gives a quantitative estimate of when point kinetics interpretation cannot be used for this method.

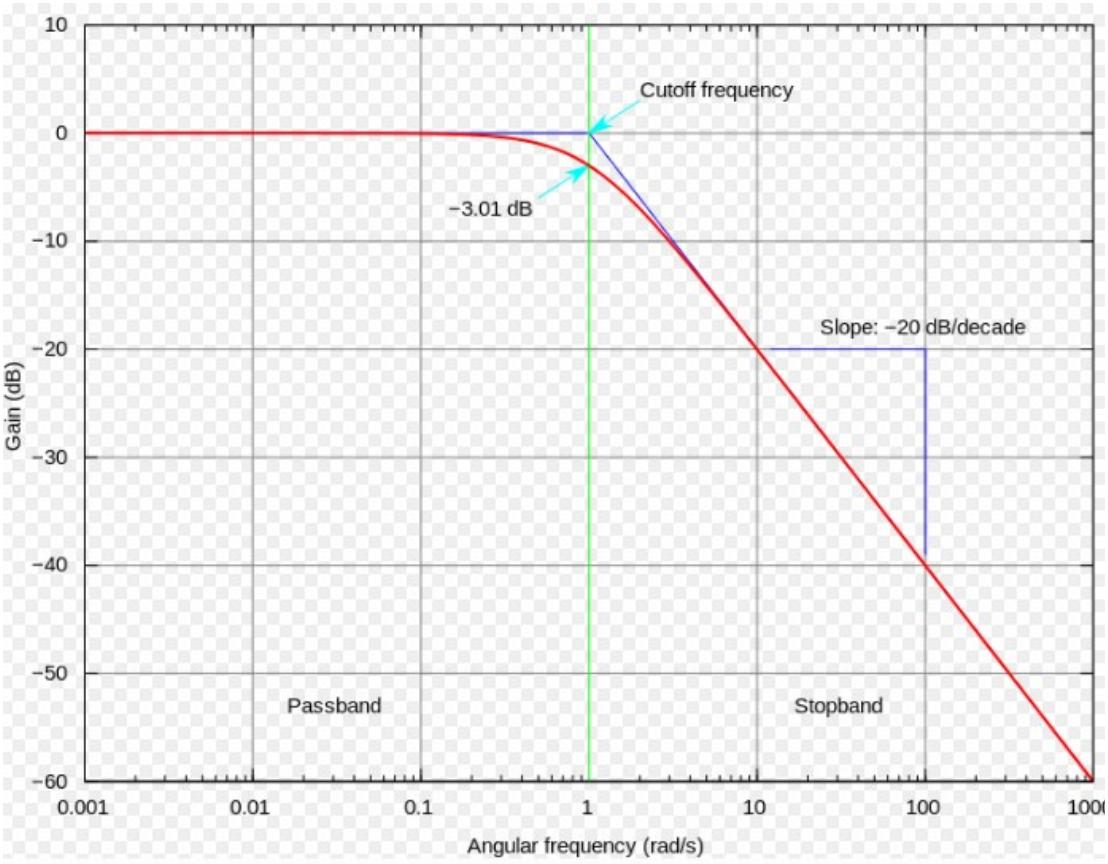

Figure B.1. Definition of the cut off or break frequency.

The prompt neutron decay constants were obtained by simultaneously fitting the APSDs of detector 2 and 3, the real and imaginary parts of the CPSDs between the detectors and the source, and the real and imaginary parts of the CPSD between the two detectors. In this simultaneously fitting, all eight functions of frequency were corrected for the frequency response of the measurement systems. The frequency response was determined in separate measurements with only the source and two detectors spaced in air. This fitting determined the break frequency (f_b) which is related to the prompt neuron decay constant (α) by the relation $\alpha = 2\pi f_b$. The measured prompt neutron decay constants presented in Table B.1 increase in magnitude as the system becomes more subcritical. For some of the configurations the prompt neutron decay constants were obtained from single mode fits of the measured spectra, while for other configurations two mode fits were performed for the measured spectra. Examination of the real and

imaginary parts of the CPSD easily reveals the presence of mode than on mode. If the real part of the CPSD is plotted as the abscissa and the imaginary part is the ordinate, single mode decay is characterized by the resulting curve being in the fourth quadrant (i.e. real part > 0 and imaginary part < 0). Some results for one configuration are given in Figure B.2 and B.3. A change of sign of either the real or the imaginary part of G_{12} signifies the presence of higher modes. The prompt neutron decay constants vary from 290 ± 9 s^{-1} at delayed critical to ~15,000 s-1 for a configuration of 289 fuel pins with 1511 ppm boron. Some results of the fitting are given in Figures B.2 and B.3 and the prompt neutron decay constants obtained from the fitted break frequency are given in Table B.1.

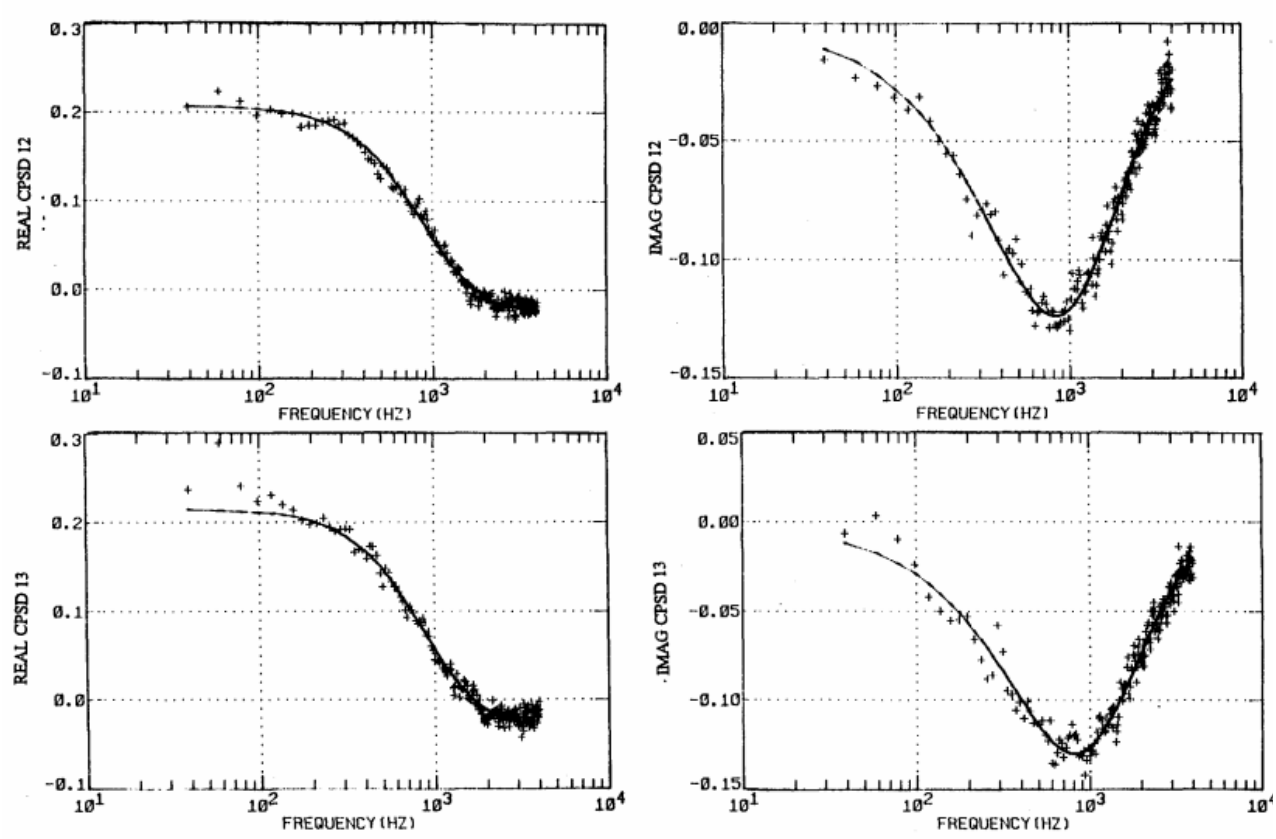

Figure B.2. Real and imaginary parts of the cross power spectral densities between the two detectors (2 and 3) and the californium source (1) for a fuel pin configuration of 4,962 fuel pins with a boron concentration of 2,386 ppm for detector 2 located at 30.4 cm SE–S–SW and detector 3 located 30.4 cm NE–N–NW (the solid lines are the results of fitting all 8 functions simultaneously).

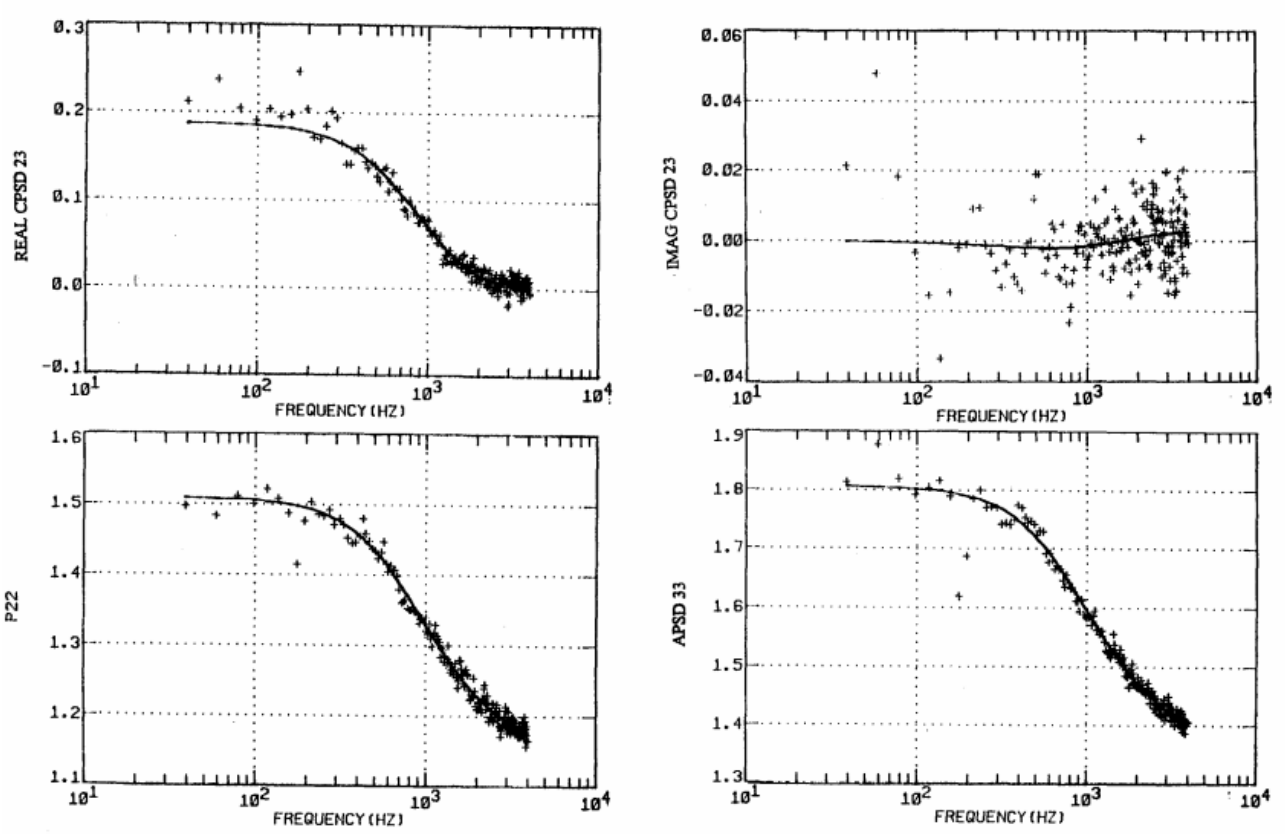

Figure B.3. Real and imaginary parts of the cross power spectral density between the two detectors (2 & 3). Auto power spectral densities for detectors 2 and 3 for a fuel pin configuration with a boron concentration of 2,386 ppm for detector 2 located at 30.4 cm SE–S–SW and detector 3 located at 30.4 cm NE–N–NW (the solid lines are the results of fitting all 8 functions simultaneously).

Table B.1. Prompt neutron decay constant from least squared fitting of cross power and auto power spectral densities.

Number of fuel pins	Boron (ppm)	Detector 2 location	Detector 3 location	Prompt neutron decay constant
4,961	1,511	all[a]	all[a]	274.7 ± 3.6[b]
4,961	1,561	30.4 S	30.4 N	622 ± 4
4,961	1,613	30.4 SE-S-SW	30.4 NE-N-NW	972 ± 4
4,961	1,765	30.4 SE-S-SW	30.4 NE-N-NW	1,910 ± 7
4,961	1,880	30.4 SE-S-SW	30.4 NE-N-NW	2,560 ± 15
4,961	1,880	30.4 S	30.4 N	2,650 ± 15
4,961	1,880	45.7 S	45.7 N	2,752 ± 22
4,961	1,880	45.7 S	45.7 N	2,737 ± 23
4,961	2,104	15.2 SE-S-SW	15.2 NE-N-NW	3,330 ± 63
4,961	2,386	30.4 SE-S-SW	30.4 NE-N-NW	5,889 ± 36
4,961	2,925	15.2 SE-S-SW	15.2 NE-N-NW	10,700 ± 3,160
4,961	3,606	30.4 SE-S-SW	30.4 NE-N-NW	13,100 ± 350
4,961	4,303	30.4 SE-S-SW	30.4 NE-N-NW	17,100 ± 1,190
3,713	1,511	30.4 SE-S-SW	30.4 NE-N-NW	892 ± 3
2,553	1,511	30.4 SE-S-SW	30.4 NE-N-NW	1,830 ± 6
2,553	1,511	45.7 SE	45.7 S	1,777 ± 18
1,281	1,511	30.4 SE-S-SW	30.4 NE-N-NW	4,210 ± 24
749	1,511	30.4 SE-S-SW	30.4 NE-N-NW	7,000 ± 75
333	1,511	30.4 SE-S-SW	30.4 NE-N-NW	11,800 ± 630
289	1,511	15.2 SE-S-SW	15.2 NE-N-NW	15,100 ± 401
289	1,511	15.2 SE-NW	15.2 NE–SW	15,400 ± 970
289	1,511	15.2 S	15.2N	15,140 ± 1,453

APPENDIX C. COMPARISON OF k_{eff} FROM THE BFNA AND CSDNA METHODS FOR THE DRAINING TANK

The break frequency values that were obtained from least-squared fitting of the auto- and cross-power spectral densities were used to determine the k_{eff} values and compared to those from the CSDNA method for the draining tank measurements. The change in the neutron lifetime for a change in the solution height was a factor of 2.1. The comparisons are given in Table C.1. The uncertainties are one standard deviation. The k_{eff} value from BFNA was normalized to that from the CSDNA method. Down to k_{eff} values of about 0.66, the values from both methods agree.

Table C.1. Comparison of inferred neutron multiplication factors of californium source-driven noise analysis with break frequency noise analysis interpretation for the draining tank measurement.

Solution Height (cm)	Break frequency sec^{-1}	k_{eff}	
		BFNA	CSDNA
29.5	1 369 ± 7[b]	0.956[b] ± 0.003	0.956' ± 0.001
29.5	1 385 ± 7	0.956[b] ± 0.003	0.956' ± 0.001
29.5	1 375 ± 7	0.956[b] ± 0.003	0.956` ± 0.001
27.6	1 819 ± 13	0.939 ± 0.004	0.940 ± 0.002
25.7	2 320 ± 9	0.921 ± 0.004	0.921 ± 0.002
23.8	2 889 ± 12	0.899 ± 0.005	0.896 ± 0.003
22.0	3 563 ± 14	0.875 ± 0.006	0.872 ± 0.004
20.2	4 327 ± 8	0.845 ± 0.007	0.845 ± 0.005
18.4	5 175 ± 20	0.814 ± 0.009	0.812 ± 0.006
16.5	6 218 ± 13	0.772 ± 0.010	0.771 ± 0.008
14.7	7 468 ± 18	0.720 ± 0.011	0.723 ± 0.011
13.1	8 955 ± 30	0.659 ± 0.013	0.662 ± 0.015
11.4	10 537 ± 31	0.605 ±0.009	0.588 ±0.021
9.9	12 325 ± 98	0.543 ± 0.014	0.522 ± 0.027
8.5	14 388 ± 143	0.478 ± 0.014	0.443 ± 0.038
7.3	16 414 ± 197	0.418 ± 0.014	0.376 ± 0.048

Note: The change in neutron lifetime for a change in solution height from 29.5 cm to a solution height of 7.3 cm was a factor of 2.1.

[a]Uncertainties are one standard deviation of the mean from the least-squares fitting of data.

[b]Assumed to be equal to the average value from the ratio of spectral densities.

APPENDIX D. MEASUREMENT RUN FILES

This appendix lists all the experimental runs and they are given in Table D.1.

Table D.1. Measurement Run Identifications.

Noise analysis run	Number of fuel pins[a]	Detector locations[b] 2 (cm)	3 (cm)	Frequency range of Fourier Analyzer (kHz)	Source location	Boron concentration (ppm)	Remarks
AA	4961	45.7S	45.7N	0.5	None	1511	
AB	4961	61.0S	61.0N	0.5	None	1511	
AC	4961	45.7S	45.7N	0.5	None	1511	
AD	4961	61.0S	61.0N	0.5	None	1511	
AE	4961	45.7S	45.7N	0.5	None	1511	Before IKRD
AF	4961	61.0S	61.0N	0.5	None	1511	Before IKRD
AG	83 4961	45.7S	45.7N	0.5	C-19(P	1511	After IKRD,1+2,Blade 2 in
AH	4961	68.6S	68.6N	0.5	C-19(P	1511	After IKRD,1+2,Blade 2 in
AI	4961	61.0S	61.0N	0.5	C-19(P	1511	
AJ	4961	68.6S	68.6N	0.5	C-19(P	1511	After IKRD 3
AK	4961	61.0S	61.0N		C-19(P	1511	Before IKRD 4
AL 8-4-83	4961	68.6S	68.6N	0.5	C-19(P	1511	
AM	4961	61.0S	61.0N	0.5	C-19(P	1511	
AN	4961	45.7S	45.7N	0.5	C-19(P)	1511	Before IKRD 5
AO	4961	45.7S	45.7N	0.5	67.9 E-19(P)	1511	After IKRD 5
AP	4961	45.7S	45.7N	0.5	67.9 E-19(P	1511	Source east
AQ	4961	45.7,	45.7,	0.5	67.9 E-19(P	1511	Source east
AR	4961	45.7S	45.7N	0.5	Top-19(P)	1511	Source top
AS	4961	45.7S	45.7N	0.5	Top-19(P)	1511	Source top
AT	4961	45.7,	45.7,	0.5	Top-19(P)	1511	Before IKRD 6
AU	4961	30.4S	30.4N	0.5	C-19(P	1561	Boron conc. change
AV	4961	45.7S	45.7N	0.5	C-19(P)	1561	Detector Traverse
AW	4961	61.0S	61.0N	0.5	C-19(P)	1561	Detector Traverse
AX	4961	61.0S	61.0N	0.5	C-19(P)	1561	Before IKRD 7
AY	4961	AllS	AllN	0.5	Top-19(P)	1561	Source at top
AZ	4961	30.4N	30.4S	0.5	Top-19(P)	1561	Before IKRD 8
BA	4961	All	All	0.5	67.9 E-19(P)	1561	Source at side
BB	4961	30.4N	30.4S	0.5	67.9 E-19(P)	1561	Source at side
BC	4961	45.7SE-S-SW	45.7NE-N-NW	1.0	C-19(P)	1613	Boron conc. change
BD	4961	45.7N	45.7S	1.0	C-19(P)	1613	Before IKRD 9
BE	4961	45.7SE-S-SW	45.7NE-N-NW	1.0	Top-19(P)	1613	Source on top
BF	4961	61.0SE-S-SW	61.0NE-N-NW	1.0	C-19(P)	1613	Source in center
BG	4961	61.0S	61.0N	1.0	C-19(P)	1613	Before IKRD 10
BH	4961	61.0SE-S-SW	61.0NE-N-NW	1.0	Top-19(P	1613	Source at top
BI	4961	30.4SE-S-SW	30.4NE-N-NW	1.0	C-19(P)	1613	Source at center
BJ	4961	30.4S	30.4N	1.0	C-19(P)	1613	
BK	4961	30.4SE-SW	30.4NE-NW	1.0	C-19(P)	1613	Before IKRD 11
BL	4961	30.4SE-S-SW	30.4NE-N-NW	2.5	C-19(P)	1765	Boron conc. change
BM	4961	30.4S	30.4N	2.5	C-19(P)	1765	1 detector
BN	4961	30.4SE-SW	30.4NE-NW	2.5	C-19(P)	1765	2 detectors
BO	4961	30.4SE-NW	30.4NE-SW	2.5	C-19(P)	1765	Before IKRD 12
BP	4961	30.4SE-S-SW	3-30.4NE-N-NW	2.5	Top-19(P)	1765	Source at top
BQ	4961	45.7SE-S-SW	3-45.7NE-N-NW	2.5	C-19(P)	1765	Source at center
BR	4961	45.7SE-S-SW	45.7NE-N-NW	2.5	C-19(P)	1765	Source at center
BS	4961	45.7SE-SW	45.7NE-NW	2.5	C-19(P)	1765	2 detectors
BT	4961	45.7S	45.7N	2.5	C-19(P)	1765	1 detector
BU	4961	45.7S	45.7N	2.5	C-19(P)	1765	1 detector
BV	4961	45.7SE-NW	45.7NE-SW	2.5	C-19(P)	1765	2 detectors
BW	4961	45.7SE-S-SW	45.7NE-N-NW	2.5	Top-19(P)	1765	Source at top
BX	4961	61.0SE-S-SW	61.0NE-N-NW	2.5	C-19(P)	1765	Source at center
BY	4961	61.0SE-SW	61.0NE-NW	2.5	C-19(P)	1765	2 detectors
BZ	4961	61.0S	61.0N	2.5	C-19(P)	1765	1 detector

Noise analysis run	Number of fuel pins[a]	Detector locations[b] 2 (cm)	3 (cm)	Frequency range of Fourier Analyzer (kHz)	Source location	Boron concentration (ppm)	Remarks
CA*	4961	30.4SE-S-SW	3-30.4NE-N-NW	2.5	C-19(P)	1880	Source at center
CB	4961	30.4SE-SW	30.4NE-NW	2.5	C-19(P)	1880	2 detectors
CC	4961	30.4S	30.4N	2.5	C-19(P)	1880	1 detector
CD	4961	30.4SE-NW	30.4NE-SW	2.5	C-19(P)	1880	2 detectors
CE	4961	45.7SE-S-SW	45.7NE-N-NW	2.5	C-19(P)	1880	3 detectors
CF	4961	45.7SE-SW	45.7NE-NW	2.5	C-19(P)	1880	2 detectors
CG	4961	45.7S	45.7N	2.5	C-19(P)	1880	1 detector
CH	4961	45.7S	45.7N	2.5	15.5W-19(P)	1880	Source traverse
CI	4961	45.7S	45.7N	2.5	30.3W-19(P)	1880	Source traverse
CJ	4961	45.7S	45.7N	2.5	30.3W-21(I)	1880	Source traverse
CK	4961	45.7S	45.7N	2.5	45.0W-21(I)	1880	Source traverse
CL	4961	45.7SW	45.7NW	2.5	45.0W-21(I)	1880	Source traverse
CM	4961	45.7S	45.7N	2.5	30.3W-21(P)	1880	Source traverse
CN	4961	45.7S	45.7N	2.5	30.3W-21(I)	1880	Source traverse
CO	4961	45.7S	45.7N	2.5	61.3W-21(I)	1880	Source traverse
CP	4961	61.0ALLS	61.0ALLN	2.5	C-21(I)	1880	All detectors
CQ	4961	61.0SE-SW	61.0NE-NW	2.5	C-21(I)	1880	2 detectors
CR	4961	SCI	SCI	2.5	C-21(I)	1880	Cf 21 current mode
CS	4961	61.0, 68.6S	61.0, 68.6N	2.5	C-21(I)	1880	2 detectors
CT	4961	2SCI	2SCI	2.5	C-21(I)	1880	Scintillators
CU	4961	3-30.4S	3-30.4N	2.5	C-21(I)	2104	Boron conc. change
CV	4961	30.4SE-SW	30.4NE-NW	2.5	C-21(I)	2104	2 detectors
CW	4961	30.4S	30.4N	2.5	C-21(I)	2104	1 detector
CX	4961	30.4SE	30.4NW	2.5	C-21(I)	2104	1 detector
CY	4961	30.4SE-NW	30.4SW-NE	2.5	C-21(I)	2104	2 detectors
CZ	4961	45.7S	45.7N	2.5	C-21(I)	2104	1 detector
DA	4961	45.7SE-SW	45.7NE-NW	2.5	C-21(I)	2104	2 detectors

Noise analysis run	Number of fuel pins[a]	Detector locations[b] 2 (cm)	3 (cm)	Frequency range of Fourier Analyzer (kHz)	Source location	Boron concentration (ppm)	Remarks
DC	4961	45.7SE-NW	45.7SW-NE	2.5	C-21(I)	2104	
DD	4961	61.0SE-S-SW	61.0NE-N-NW	2.5	C-21(I)	2104	
DE	4961	61.0SE-SW	61.0NE-NW	2.5	C-21(I)	2104	2 detectors
DF	4961	61.0, 68.6S	61.0, 68.6N	2.5	C-21(I)	2104	2 detectors
DG	4961	4S	4N	2.5	Top-21(I)	2104	Source at top
DH	4961	4S	4N	2.5	Top-21(I)	2104	Source at top
DI	4961	4S	4N	2.5	67.9E-21(I)	2104	Source at side
DJ	4901	30.4-3S	30.4-3N	2.5	C-22(I)	2104	3 detectors
DK	4901	30.4S	30.4N	2.5	C-22(I)	2104	1 detector
DL	4961	15.2-3S	15.2-3S	2.5	C-19(P)	2104	3 detectors
DM	4961	15.2SE-SW	15.2NE-NW	2.5	C-19(P)	2104	2 detectors
DN	4961	4S	4N	2.5	67.9E-22(I), W-21(I)	2104	2 sources
DO	4961	4S	4N	2.5	155E-22, 15.5W-21(I)	2104	2 sources
DP	4961	15.2SE-S-SW	15.2NE-N-NW	5.0	C-19(P)	2386	Boron conc. change
DQ	4961	15.2SE-SW	15.2NE-NW	5.0	C-19(P)	2380	2 detectors
DR	4961	15.2S	15.2N	5.0	C-19(P)	2386	1 detector
DS*	4961	30.4SE-S-SW	30.4NE-N-NW	5.0	C-19(P)	2386	3 detectors
DT	4961	30.4SE-SW	30.4NE-NW	5.0	C-19(P)	2386	2 detectors
DU	4961	30.4S	30.4N	5.0	C-19(P)	2386	1 detector
DV	4961	30.4SE-S-SW	30.4NE-N-NW	5.0	C-22(I)	2386	3 detectors
DW	4961	30.4SE-SW	30.4NE-NW	5.0	C-22(I)	2386	2 detectors
DX	4961	30.4S	30.4N	5.0	C-22(I)	2386	1 detector
DY*	4961	30.4SE-S-SW	30.4NE-N-NW	5.0	C-21(I)	2386	3 detectors
DZ	4961	30.4SE-SW	30.4SE-SW	5.0	C-21(I)	2386	2 detectors
EA	4961	30.4S	30.4N	5.0	C-21(I)	2386	1 detector

Noise analysis run	Number of fuel pins[a]	Detector locations[b] 2 (cm)	3 (cm)	range of Fourier Analyzer (kHz)	Source location	Boron concentration (ppm)	Remarks
EE	4961	45.7S	45.7N	5.0	15.5W-21(I)	2386	Source traverse
EF	4961	45.7S	45.7N	5.0	30.3W-21(I)	2386	Source traverse
EG	4961	45.7S	45.7W	5.0	30.3W-21(I)	2386	Source traverse
EH	4961	45.7S	45.7N	5.0	45.0W-21(I)	2386	Source traverse
EI	4961	45.7S	45.7N	5.0	45.0W-21(I)	2386	Source traverse
EJ	4961	4S	4N	5.0	C-21(I)	2386	4 detectors
EK	4961	61.0SE-S-SW	61.0NE-N-NW	5.0	C-21(I)	2386	3 detectors
EL	4961	61.0SE-S-SW	61.0NE-N-NW	5.0	C-21(I)	2386	3 detectors
EM	4961	4S	4N	5.0	15.5 Top2(I)	2386	2 sources top
EN	4961	4S	4N	5.0	15.5 Top2(I)	2386	2 sources top
EO	4961	4S	4N	5.0	15.5 Top2(I)	2386	2 sources top
EP	4961	4S	4N	5.0	67.8E-67.8W(I)	2386	2 source traverse
EQ	4961	4S	4N	5.0	67.8E-67.8W(I)	2386	2 source traverse
ER	4961	4S	4N	5.0	67.8E-67.8W(I)	2386	2 source traverse
ES	4961	4S	4N	5.0	61.3E-61.3W(I)	2386	2 source traverse
ET	4961	4S	4N	5.0	61.3E-61.3W(I)	2386	2 source traverse
EU	4961	30.4SE-S-SW	30.4NE-N-NW	5	C-21(I)	2925	Boron conc. change
EV	4961	30.4SE-S-SW	30.4NE-N-NW	10	C-21(I)	2925	3 detectors
EW	4961	30.4SE-SW	30.4NE-NW	5	C-21(I)	2925	2 detectors
EX	4961	30.4S	30.4N	5	C-21(I)	2925	1 detector
EY	4961	45.7SE-S-SW	45.7NE-N-NW	5	C-21(I)	2925	3 detectors
EZ	4961	45.7SE-SW	45.7NE-NW	5	C-21(I)	2925	2 detectors
FA	4961	45.7S	45.7N	5	C-21(I)	2925	1 detector
FB	4961	4S	4N	5	C-21(I)	2925	4 detectors
FC	4961	4S	4N	5	C-22(I)	2925	4 detectors
FD	4961	4S	4N	5	C-22(I)	2925	1 detector
FE	4961	4S	4N	5	C-22(I)	2925	1 detector
FF	4961	15.2SE-S-SW	15.2NE-N-NW	5	C-19(P)	2925	3 detectors

Noise analysis run	Number of fuel pins[a]	Detector locations[b] 2 (cm)	3 (cm)	Frequency range of Fourier Analyzer (kHz)	Source location	Boron concentration (ppm)	Remarks
FG	4961	15.2SE-SW	15.2NE-NW	5	C-19(P)	2925	2 detectors
FH	4961	15.2S	15.2N	5	C-19(P)	2925	1 detector
FI	4961	45.7S	45.7N	5	C-22(I)	2925	1 detector
FJ	4961	30.4SE-S-SW	30.4NE-N-NW	10	C-22(I)	3606	Boron conc. change
FK	4961	30.4SE-SW	30.4SE-SW	10	C-22(I)	3606	2 detectors
FL	4961	30.4S	30.4N	10	C-22(I)	3606	1 detector
FM	4961	45.7SE-S-SW	45.7NE-N-NW	10	C-22(I)	3606	3 detectors
FN	4961	45.7S	45.7N	10	C-22(I)	3606	1 detector
FO	4961	4S	4N	10	C-22(I)	3606	Dry lattice
FP	4961	4S	4N	10	C-22(I)	3606	detector failed (#8)
FQ	4961	4S	3N	10	C-22(I)	3606	Water in, 4 detectors
FR	4961	4S	3N	10	C-22(I)	3606	Dry lattice, 4 detectors
FS	4961	4S	3N	10	C-22(I)	3606	Dry lattice, 4 detectors
FT	4961	4S	3N	10	C-22(I)	3606	Water in, 4 detectors
FU	4961	4S	3N	10	C-22(I)	3606	Water in, 4 detectors
FV	4961	4S	3N	10	C-22(I)	3606	Dry-contamination of FR
FW	4961	15.4S	15.4N	10	C-22(I)	3606	Current pulse comparison
FX	4961	15.4SE-SW	15.4NE-NW	10	C-22(I)	3606	Current pulse comparison
FY	4961	15.4E-SW	15.4NE-NW	10	C-19(P)	3606	Current pulse comparison
FZ	4961	15.4S	15.4N	10	C-19(P)	3606	Current pulse comparison
GA	4961	15.4SE-S-SW	15.4NE-N-NW	10	C-19(P)	4303	Boron conc. change
GB	4961	15.4SE-SW	15.4NE-NW	10	C-19(P)	4303	2 detectors
GC	4961	15.4S	15.4N	10	C-19(P)	4303	1 detector
GD	4961	30.4SE-S-SW	30.4NE-N-NW	10	C-22(I)	4303	3 detectors
GE	4961	30.4SE-SW	30.4NE-NWW	10	C-22(I)	4303	2 detectors

Noise analysis run	Number of fuel pins[a]	Detector locations[b] 2 (cm)	Detector locations[b] 3 (cm)	Frequency range of Fourier Analyzer (kHz)	Source location	Boron concentration (ppm)	Remarks
GI	4961	4S	4N	5	61.3-22(I)	2439	Source on side
GJ	3713	30.4SE-S-SW	30.4NE-N-NW	1	C-19(P)	1511	Boron and fuel change
GK	3713	30.4SE-SW	30.4NE-NW	1	C-19(P)	1511	2 detectors
GL	3713	30.4S	30.4W	1	C-19(P)	1511	1 detector
GM	3713	30.4SE	30.4NE	1	C-19(P)	1511	1 detector
GN	3713	45.7SE-S-SW	45.7NE-N-NW	1	C-19(P)	1511	3 detectors
GO	3713	45.7SE-SW	45.7NE-NW	1	C-19(P)	1511	2 detectors
GP	3713	45.7SE-NW	45.7SW-NE	1	C-19(P)	1511	2 detectors
GQ	3713	45.7S	45.7N	1	C-19(P)	1511	1 detector
GR	3713	61.0SE-S-SW	61.0NE-N-NW	1	C-19(P)	1511	3 detectors
GS	3713	61.0SE-SW	61.0NE-NW	1	C-19(P)	1511	2 detectors
GU	3713	61.0S	61.0N	1	C-19(P)	1511	IKRD 13
GV	2553	30.4SE-S-SW	30.4NE-N-NW	2.5	C-19(P)	1511	Smaller array
GW	2553	30.4SE-SW	30.4NE-NW	2.5	C-19(P)	1511	2 detectors
GX	2553	30.4S	30.4N	2.5	C-19(P)	1511	1 detector
GY	2553	45.7SE-S-SW	45.7NE-N-NW	2.5	C-19(P)	1511	3 detectors
GZ	2553	45.7SE-SW	45.7NE-NW	2.5	C-19(P)	1511	2 detectors
HA	2553	45.7S	45.7N	2.5	C-19(P)	1511	1 detector
HB	2553	45.7SE-NW	45.7SW-NE	2.5	C-19(P)	1511	2 detectors
HC	2553	45.7S-SW	45.7N-NE	2.5	C-19(P)	1511	2 detectors
HD	2553	45.7SE	45.7S	2.5	C-19(P)	1511	1 detector
HE	2553	45.7SE	45.7SW	2.5	C-19(P)	1511	IKRD 14
HF	1281	30.4SE-S-SW	30.4NE-N-NW	2.5	C-19(P)	1511	Smaller array
HG	1281	30.4SE-SW	30.4NE-NW	2.5	C-19(P)	1511	2 detectors
HH	1281	30.4S	30.4N	2.5	C-19(P)	1511	1 detector
HI	1281	30.SE-NW	30.4SW-NE	2.5	C-19(P)	1511	2 detectors
HJ	1281	30.4S-SW	30.4N-NE	2.5	C-19(P)	1511	1 detector
HK	1281	15.2SE-S-SW	15.2NE-N-NW	2.5	C-19(P)	1511	3 detectors

Noise analysis run	Number of fuel pins[a]	Detector locations[b] 2 (cm)	Detector locations[b] 3 (cm)	Frequency range of Fourier Analyzer (kHz)	Source location	Boron concentration (ppm)	Remarks
HL	1281	15.2SE-SW	15.2NE-NW	2.5	C-19(P)	1511	2 detectors
HM	1281	15.2S	15.2N	2.5	C-19(P)	1511	1 detector
HN	1281	15.2SE-NW	15.2SW-NE	2.5	C-19(P)	1511	2 detectors
HO	1281	15.2S-SW	15.2N-NE	2.5	C-19(P)	1511	1 detector
HP	1281	45.7SE-S-SW	45.7NE-N-NW	2.5	C-19(P)	1511	3 detectors
HQ	1281	45.7SE-SW	45.7NE-NW	2.5	C-19(P)	1511	2 detectors
HR	1281	45.7S	45.7W	2.5	C-19(P)	1511	1 detector
HS	1281	45.7S-SW	45.7N-NE	2.5	C-19(P)	1511	2 detectors
HT	749	30.4SE-S-SW	30.4NE-N-NW	5	C-19(P)	1511	Smaller array
HU	749	30.4SE-SW	30.4NE-NW	5	C-19(P)	1511	2 detectors
HV	749	30.4S	30.4N	5	C-19(P)	1511	1 detector
HW	749	30.4S-SWW	30.4N-NE	5	C-19(P)	1511	2 detectors
HX	749	30.4SE-NW	30.4SW-NE	5	C-19(P)	1511	2 detectors
HY	749	15.2SE-S-SW	15.2NE-N-NW	5	C-19(P)	1511	3 detectors
HZ	749	15.2SE-SW	15.2NE-NW	5	C-19(P)	1511	2 detectors
IA	749	15.2S	15.2N	5	C-19)P)	1511	1 detector
IB	749	15.2S-SW	15.2N-NE	5	C-19(P)	1511	2 detectors
IC	333	15.2SE-S-SW	15.2NE-N-NW	5	C-19(P)	1511	Smaller array
ID	333	15.2SE-S-SW	15.2NE-N-NW	5	C-19(P)	1511	3 detectors
IE	333	15.2S	15.2N	5	C-19(P)	1511	1 detector
IF	333	15.2SE-SW	15.2NE-NW	5	C-19(P)	1511	2 detectors
IG	333	15.2SE-NW	15.2SW-NE	5	C-19(P)	1511	2 detectors
IH	333	15.2S-SW	15.2N-NE	5	C-19(P)	1511	1 detector
II	333	30.4S	30.4N	5	C-19(P)	1511	3 detectors
IJ	333	30.4 SE-S-SW	30.4NE-N-NW	5	C-19(P)	1511	2 detectors
IK	333	30.4SE-SW	30.4NE-NW	5	C-19(P)	1511	3 detectors
IL	269	15.2SE-S-SW	15.2NE-N-NW	5	C-19(P)	1511	PWR single element
IM	269	15.2SE-SW	15.2NE-NW	5	C-19(P)	1511	2 detectors

Noise analysis run	Number of fuel pins-	Detector locations- 2 (cm)	3 (cm)	Frequency range of Fourier Analyzer (kHz)	Source location	Boron concentration (ppm)	Remarks
IN	269	15.2S	15.2N	5	C-19(P)	1511	1 detector
IO	269	15.2SW	15.2NE	5	C-19(P)	1511	1 detector
IP	269	15.2SE-NW	15.2SW-NE	5	C-19(P)	1511	2 detectors
IQ	269	15.2S-SW	15.2N-NE	5	C-19(P)	1511	2 detectors
IR	269	30.4SE-S-SW	30.4NE-N-NW	5	C-19	1511	3 detectors
IS	269	30.4SE-SW	30.4NE-NW	5	C-19(P)	1511	2 detectors

APPENDIX E. CALIFORNIUM SOURCE-DRIVEN-NOISE ANALYSIS

E.1 BACKGROUND

This appendix presents a review of the source noise analysis method and its original development and present status. This method has its origins in time-correlation-function measurement, which is the time distribution of counts in one detector with respect to a previous count in the same or another detector. This was first suggested by Bruno Rossi during the Manhattan Project and is known as the one- or two-detector Rossi-α measurement [E.1.]. Because it requires two counts, the measurement depends on the square of the detection efficiency. In 1968, californium was deposited on one plate of a parallel plate ionization chamber and its spontaneous fission provided a timing signal as to when neutrons were emitted. Therefore, the use of californium in this way provided the basis for a randomly pulsed neutron source [E.2.], which was used to measure the time distribution of counts in a detector with respect to a count in the californium ionization chamber. This measurement acquired data much faster than the Rossi-α because it depended on the detection efficiency and not its square, and the efficiency for counting spontaneous fission of californium was near 100%.

In 1975, the author joined the research group doing reactor noise [E.3] measurements in the frequency domain rather than the time domain. These measurements had some advantage that when the fission rates were so high that fission chains overlapped and could not be distinguished in the time domain. The auto and cross-power spectral densities in the frequency domain are just the Fourier transform of the autocorrelation function and the cross-correlation functions in the time domain. These frequency domain measurements had been developed for reactors operating at high power. This method was designated as the californium source-driven noise analysis and was used from about 1975 to 2000 to measure the subcriticality at eight US Department of Energy (DOE) facilities [E.4]. In these measurements, the californium source ionization chamber and two detectors were used. This technique measured a ratio of spectral densities that was independent of detection efficiency and thus avoided the problems of neutron source multiplication methods [E.5], which had been used for decades to monitor the approach to critical in critical facilities and in the initial startup of reactors. In about 1984, the first-time domain measurements were performed with nuclear weapons/components/highly enriched uranium metal using a timed tagged ionization chamber, and through the 1980s and 1990s, the Nuclear Materials Identification System (NMIS) was developed. The number of detectors increased to five. Since the fission chain decay was so rapid in these systems and these systems were subcritical, most of the analysis used the time domain measurements where smaller californium sources were used. However, the frequency analysis result capability was maintained in the NMIS software. Mihalczo, Mullens, Mattingly, and Valentine (2000) provide a physical description of the signatures acquired by NMIS [E.6]. The use of a time-tagged californium ionization chamber with its isotropic emission of neutron-created background problems for some measurements. In 2004, some analysis by James Mullens [E.7] indicated that with a time and directionally tagged neutron generator, the NMIS system could be expanded to perform neutron imaging. The time and directional tagging were accomplished by detecting the alpha particle from the deuterium-tritium (DT) reaction that is emitted ~180° from the neutron emission [E.8]. The NMIS software for acquiring (DAUI) and interpreting (IDAS) data was modified to multiplex signals depending on their width. The NMIS capability at that time was ten input channels capable of eight or more detectors per channel. This allowed using a row of 16 alpha pixels to define a fan beam of neutron cones, each with a separate direction that can be used for imaging, and using a radial arc of 32 detectors that can be used for imaging. This imaging work was originally supported by the Y-12 National Security complex and later by the U.S. DOE Office of Nuclear Verification. In addition, NMIS employed eight additional large detectors that could be used for active and passive time correlation measurements. The U.S. DOE Office of Nuclear Verification then supported a more friendly treaty usable system designated as the Fieldable Nuclear Material Identification System [E.9]. In 2006, a more advanced highly pixelated system was developed by Paul Hausladen and coworkers [E.10].

E.2 CALIFORNIUM SOURCE-DRIVEN NOISE ANALYSIS METHOD

This method was originally developed in 1975 for subcriticality determinations for three detectors—a time-tagged californium source and two detectors. The development of the equations for this method is given in the literature [E.11].

E.3 NOISE EQUIVALENT SOURCE

The point kinetics equations presented use the ORNL version of the noise equivalent source. Another alternate version of the noise equivalent source was developed by Akcasu and others [E.12]. This latter version has a better theoretical foundation. However, for highly subcritical systems, its use results in overestimation of the neutron multiplication. In 1990, researchers at Knolls Atomic Power Laboratory (KAPL) performed a completely independent analysis and compared the results of interpretation of measurements by both methods [E.13]. Basically, at neutron multiplication factors above 0.80, both point kinetics methods give similar results. This will be illustrated in subsequent sections of this appendix.

E.4 HIGHLY ENRICHED URANYL NITRATE SOLUTION TANK EXPERIMENT

A photograph of the tank that contained uranyl nitrate solution is given in Figure E.1. The measurements were performed with external plastic scintillation detectors detecting leakage neutrons above 1 MeV and gamma rays and external ^{3}He proportional counters detection at the lower energy spectrum of leakage neutrons. These results for measurements as a function of solution height, which are a ratio of spectral densities that can be interpreted to obtain the neutron multiplication factor, are shown in Table E.1 and in Figures E.2 and E.3. The results show the agreement with calculated neutron multiplication factors.

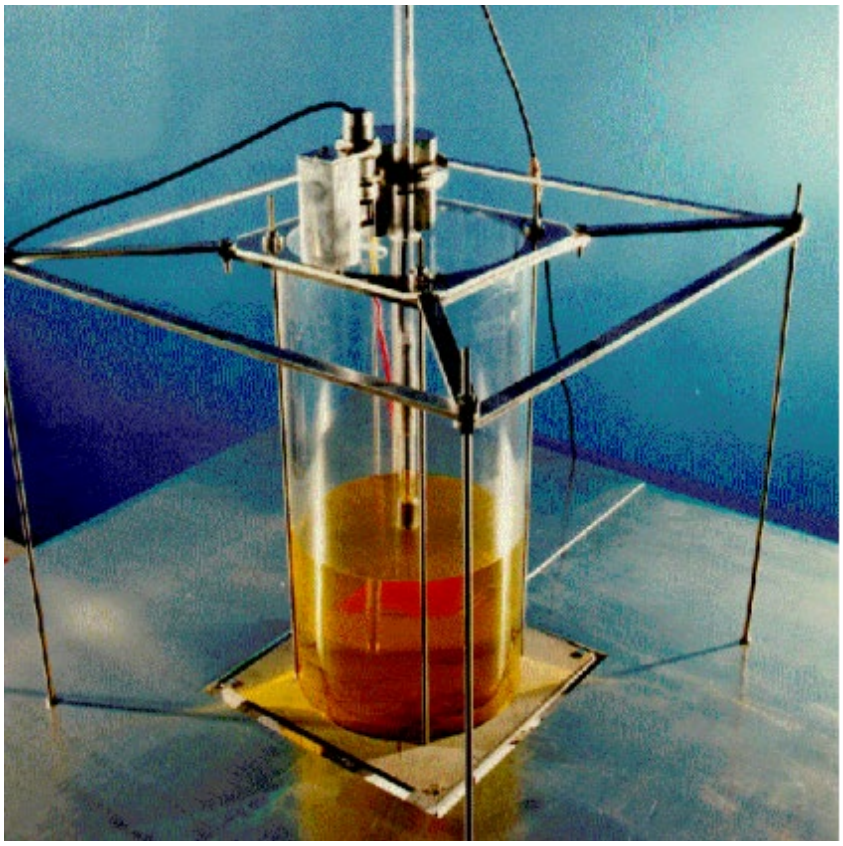

Figure E.1. Highly enriched uranyl nitrate solution tank without external detectors and the californium source at the top of the solution (solution color distorted from actual yellow by red tape on the table behind the tank).

Table E.1. Measured ratios of spectral densities at low frequencies and neutron multiplication factors from static measurement with the source at the bottom of the solution.

Solution Height (cm)	Ratio of Spectral Densities[a]		Neutron Multiplication Factors, k_{eff}		Number of Data Blocks (10^3)
	^{3}He Detectors (10^{-4})	Scintillators (10^{-4})	^{3}He Detectors	Scintillators	
29.2	453 ± 12 (5)	436 ± 5 (2)	0.952 ± 0.002	0.954 ± 0.001	20
25.8	767 ± 40 (5)	774 ± 20 (2)	0.924 ± 0.005	0.923 ± 0.003	20
20.3	1590 ± 20 (5)	1616 ± 10 (6)	0.853 ± 0.005	0.850 ± 0.005	20
15.3	2896 ± 90 (5)	2843 ± 10 (10)	0.732 ± 0.015	0.738 ± 0.010	40
10.1	4508 ± 90 (5)	4477 ± 60 (10)	0.535 ± 0.030	0.540 ± 0.027	20
9.8	---	4723 ± 60 (10)	---	0.505 ± 0.030	7
9.0	---	4960 ± 60 (10)	---	0.472 ± 0.035	100
7.5	---	5293 ± 210 (10)	---	0.414 ± 0.055	40
6.5	---	5650 ± 60 (10)	---	0.346 ± 0.049	60
5.7	---	5943 ± 360 (10)	---	0.278 ± 0.097	55

[a]Values in parentheses are the upper limit of the frequency range in kilohertz over which the ration was averaged. The precision given is one standard deviation of the mean. Uncertainties in the neutron multiplication factor are from the statistical precision of the ratio of spectral densities and the uncertainties in the parameters required to infer the neutron multiplication factor.

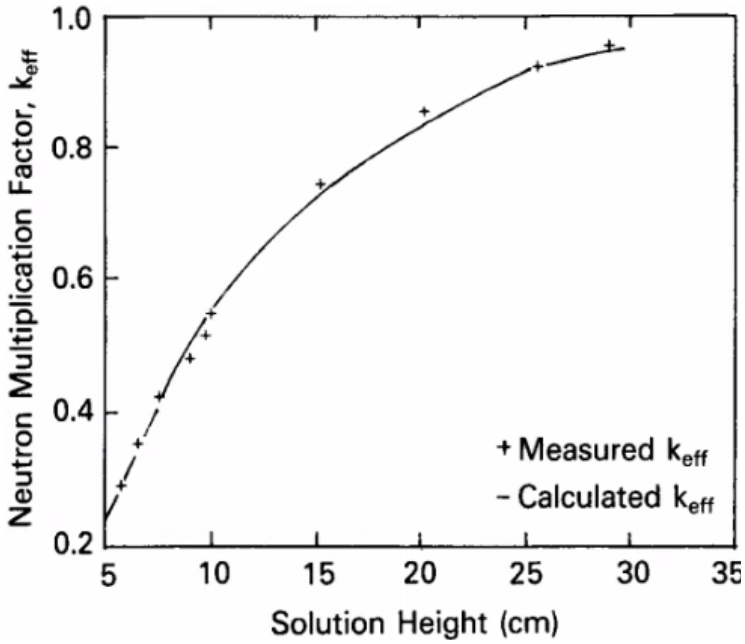

Figure E.2. Comparison of neutron multiplication factors obtained for the author's formulation of detection effects from static measurement with two ^{3}He proportional counters adjacent to the tank detecting leakage neutrons and with the source at the bottom of the tank.

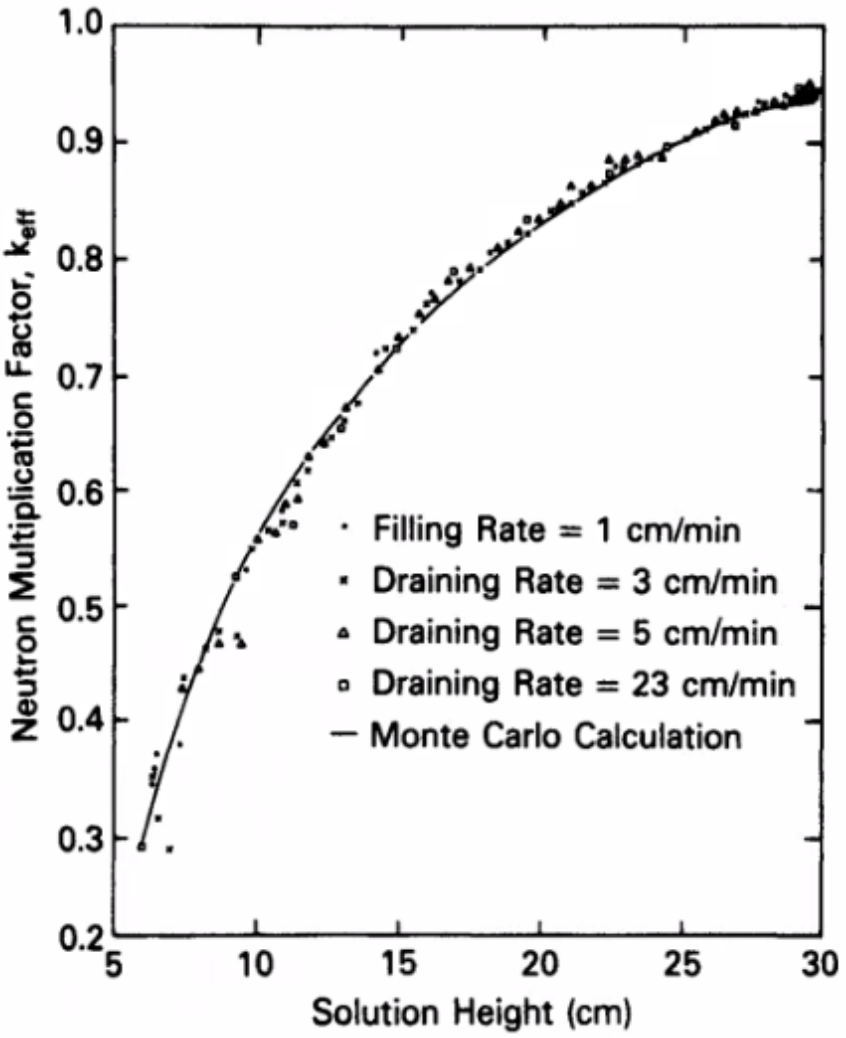

Figure E.3. Comparison of neutron multiplication factors obtained for the author's formulation of detection effects from dynamic measurement with two fast plastic scintillators adjacent to the tank detecting leakage neutrons and gamma rays and the californium source at the bottom of the tank with calculations.

Note, the measured ratio is the same as predicted by the theory for the ^{3}He proportional counters detecting lower-energy neutron spectrum neutrons and fast plastic scintillators detecting gamma rays and fast neutrons. Both these systems are detecting leakage neutron, and the scintillators are also detecting gamma rays. In fact, calculations have shown that most plastic scintillator coincidences involve only one neutron (private communication report from P. M. Keates, UK, to J. Mihalczo, Oak Ridge National Laboratory, 2019, available from John Mihalczo).

The measured and the calculated neutron multiplication factors are in excellent agreement. The neutron multiplication factors from the dynamic measurement as the tank was drained with the fast plastic scintillators and the californium source on the bottom of the tank are compared with calculations in Figure E.3.

For all draining rates, the measured neutron multiplication factors agree, they also agree with the calculations.

E.5 INTERPRETATIONS BY KNOLLS ATOMIC POWER LABORATORY USING BOTH POINT KINETICS FORMULATIONS AND COMPARISON WITH CALCULATIONS

A report by Sutton and others at Knolls Atomic Power Laboratory (KAPL) [DE13] also evaluated the ratio of spectral densities to obtain, using both the author's point kinetics formulations independent of Oak Ridge National Laboratory (ORNL) (i.e., all the necessary parameters to infer the neutron multiplication factor were obtained by Sutton and coauthors independent of ORNL for the ORNL interpretation). They also calculated the neutron multiplication factor by the KAPL Monte Carlo code (RACER) and compared to the two point kinetics formulations of interpretation of the ratio of spectral densities. Their calculated neutron multiplication factors agreed with their interpretation using the ORNL formulation. The interpretation using the formulation of KAPL and others gave neutron multiplication factors that were much higher than those from the author's interpretation at the low neutron multiplication factor values. These comparisons are presented in the Figure E.4. At a solution height of 4 in., the Mihalczo–Paré formulation gave a k_{eff} of 0.56 compared to 0.69 for the KAPL interpretation using Sutton's formulation. RACER Monte Carlo–calculated neutron multiplication factors agree with the author's formulation of the noise equivalent source formulation. At neutron multiplication factors above 0.85, the inferred neutron multiplication from both point kinetics formulations are essentially the same.

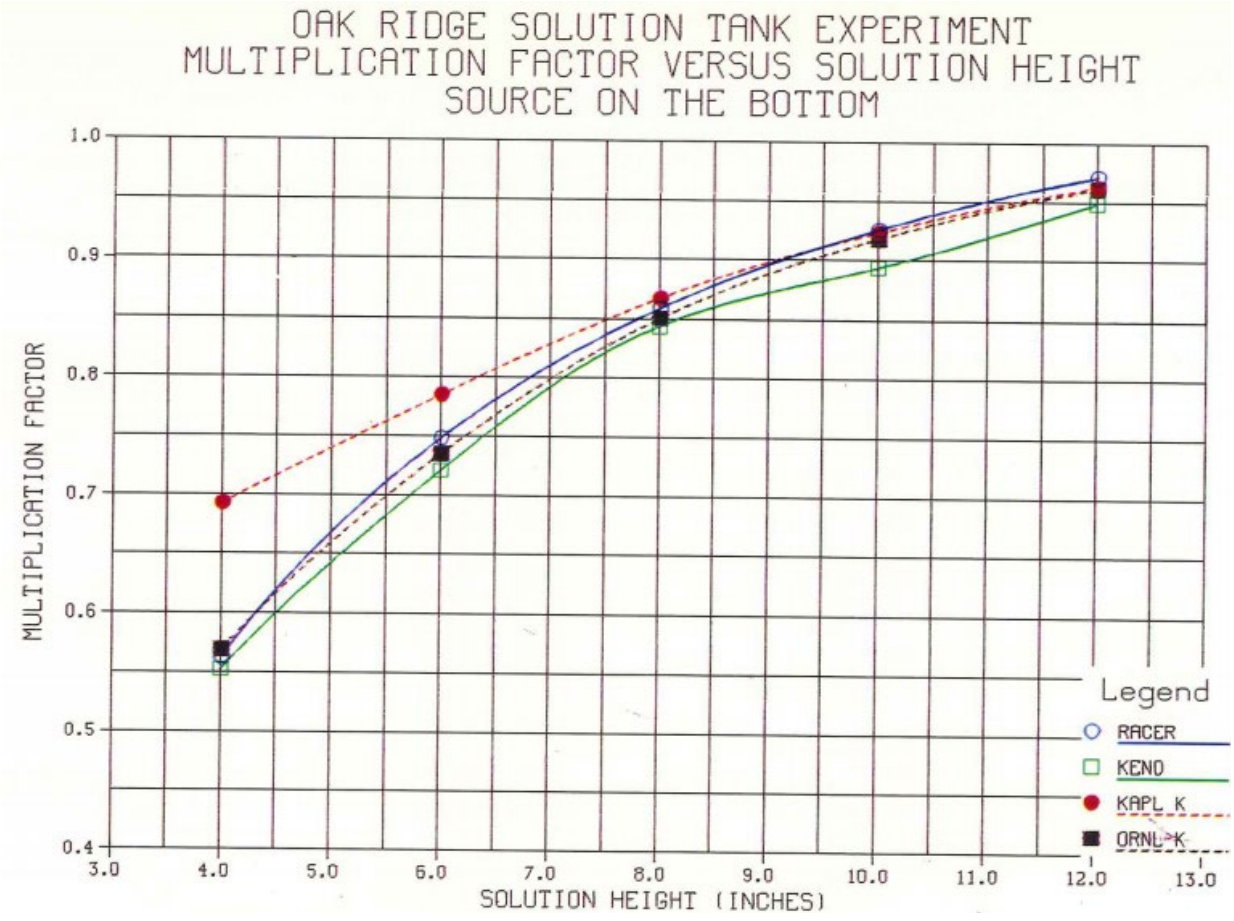

Figure E.4. Comparison of neutron multiplication factors from RACER Monte Carlo calculations with the two formulations. (Red circles are KAPL interpretation using the Akcasu/Stolle formulation, and black boxes are KAPL'S formulation using the author's formulation.)

At low neutron multiplication factors, the interpretation using the KAPL formulation gives results that do not agree with the RACER calculations. For a solution height of 4 in., the Akcasu-Stolle formulation

gives a neutron multiplication factor of 0.69, and the RACER gives 0.56. The disagreement increases as the neutron multiplication decreases and starts below the k_{eff} of 0.85.

E.6 HIGHLY ENRICHED URANYL NITRATE SOLUTION TANK EXPERIMENT

A californium source-driven noise analysis (CSDNA) measurement was performed with tank of uranyl nitrate solution [E.14]. The solution concentration of uranium (93.16 wt. % ^{235}U) in the uranyl nitrate solution was varied in 16 steps from 13.70 grams of ^{235}U per liter to 0.325 grams per liter and then 0.0 (water). To minimize the handling hazard, the solution had no free acid content. The inside diameter of the 0.32 cm thick stainless-steel tank was 76.1 and the inside height was 91.4 cm. The tank had a bottom thickness of 1.27 cm with a 1.27 cm thick plastic lid. The height of the solution was 76.2 cm. The neutron multiplication factor, k_{eff}, varied from 0.91 to 0.0. CSDNA measurements (~160) were performed at each solution concentration with a variety of detectors, detector locations, and source locations. In solution two, ^{3}He proportional counters in aluminum tubes were used and external to the tank, and plastic and liquid scintillators.

The results of the interpretation of the ratio of spectral densities from these measurements with both interpretations of the measurements are given in Figure E.5. Again, the Akcasu–Stolle formulation give higher neutron multiplication factors at low values that are much higher than those with the Mihalczo–Paré formulation, where the latter agrees with the calculations. For example, at a solution concentration of 4.45 g ^{235}U per liter, the k_{eff} value of 0.45 from the Mihalczo–Paré formulation agrees quite well with the calculations, whereas the alternate formulation gives a k_{eff} value of 0.585.

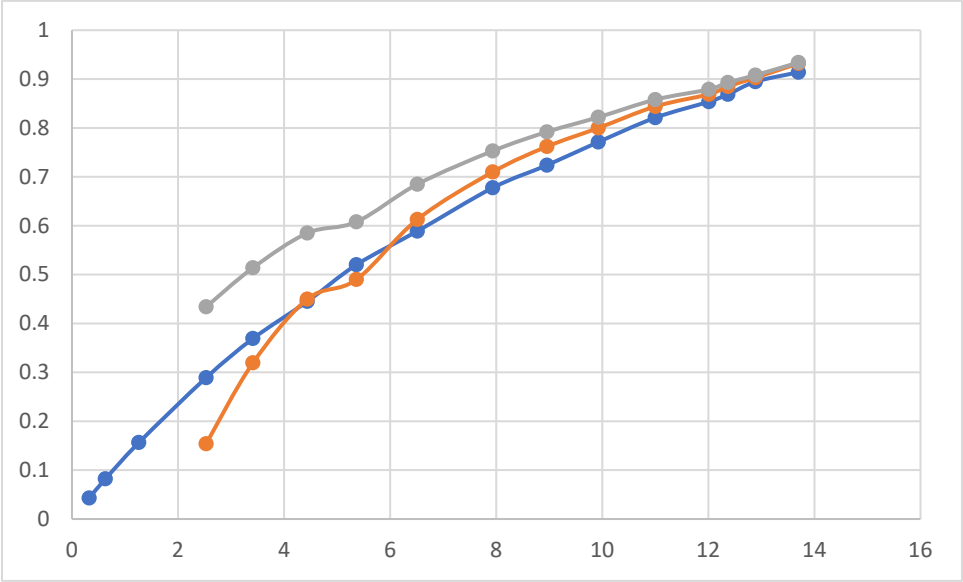

Figure E.5. Neutron multiplication factors from ratios of spectral densities with both formulations compared with calculations. (Red = Mihalczo–Paré formulation, gray = Akcasu–Stolle formulation, and blue = calculations.)

A more general model has been used to determine the neutron multiplication factor from the measured results. The Monte Carlo method can be used to directly calculate the ratio of spectral densities and its uncertainty. This avoids the use of point kinetics and replaces it with a very general method that does not have the limitations of the point kinetics model. Some examples of this use of the more general model is given in Nuclear Energy Agency evaluate criticality safety benchmarks SUB-HEU-SOL-THERM-001 and SUB-HEU-Sol-THERM-002 [Ref E.15 and E.16].

REFERENCES

E.1. John D. Orndoff, "Prompt Neutron Periods of Metal Critical Assemblies," *Nuc. Sci. Eng.*, **2**, no. 4, 450–460 (1957).

E.2. J. T. Mihalczo, "The Use of Californium-252 as a Randomly Pulsed Neutron Source for Prompt Neutron Decay Measurements," *Nucl. Sci. Eng*., **53**, no. 4, 393–414 (1974).

E.3. J. T. Mihalczo and V. K. Paré, "Theory of Correlation Measurement in Time and Frequency Domains with ^{252}Cf," *Ann. Nucl. Energy*, **2**, 97–105 (1975). [OSTI #4243449]

E.4. V. K. Paré and J. T. Mihalczo, "Reactivity from Power Spectral Density Measurements with Californium-252," *Nucl. Sci. Eng*., **56**, no. 2, 213–218 (1975).

E.5. J. T. Mihalczo, A Review of Methods for Treatment of Source Effects in the Modified Source Multiplication Method for Monitoring the Reactivity in Refueling the CRBR, ORNL-5568, Union Carbide Corp. Nuclear Division, Oak Ridge National Laboratory, September 1979. [OSTI #5984287]

E.6. J. T. Mihalczo, J.A. Mullens, J. K. Mattingly, and T. E. Valentine, "Physical Description on Nuclear Materials Identification System (NMIS) Signatures," *Nucl. Instrum. Methods Phys. Res., Sect. A*, **450**, nos. 2–3), 531–555 (Amsterdam Elsevier Science BV) (2000).

E.7. J. A. Mullens, J. T. Mihalczo, P. Bingham, "Neutron and Gamma Ray Imaging for Nuclear Materials Identification", Proc. of INMM 45th Annual Meeting, Northbrook, II, (July 2004).

E.8. D. Koltick, S. Kane, J. Mihalczo, S. McConchie, E. Mace, and M. Lvovsky, "Production of an Associated Particle Neutron Generator with ZnO:Ga Alpha-Detector," *IEEE SORMA West,* (Berkeley, CA) (June 2008).

E.9. D. Archer, C. Britton, Jr., N. Bull, M. Emery, M. Ericson, L. Fabris, E. Farquhar, S. Frank, D. Hurst, R. Lind, S. McConchie, J. Mihalczo, J. Mullens. E. Sword, and J. Radle, "The Imaging Detector Subsystem Electronics of the Fieldable Nuclear Materials Identification System (FNMIS)," *IEEE 2012 Nuclear Science Symposium* (Anaheim, California) (October 2012).

E.10. Paul Hausladen, Matthew Blackston, James Mullens, John Mihalczo "Multimodal Imaging with Tagged Fast Neutrons for Material Identification" *Presentation 2012, CAARI 2012, Aug 05, 2012-Aug 10, 2012, Ft. Worth, Texas (Aug 2012).*

E.11. J. T. Mihalczo, E. D. Blakeman, G. E. Ragan, E. B. Johnson, and Y. Hachiya, "Dynamic Subcriticality Measurements Using the ^{252}Cf-Source-Driven Noise Analysis Method," *Nucl. Sci. Eng.*, **104**, no. 4, 314–338 (1990).

E.12. A. Z. Akcasu and A. Stolle, "Langevin Equation Approach to Reactor Noise Analysis: Stochastic Transport Equation," *Nucl. Sci. Eng.* **113**, no. 1, 31–55 (1993).

E.13. J. P Weinman and M. R. Mendelson, "KAPL Monte Carlo Analysis of Subcritical Reactivity Measurements in the Oak Ridge Solution Tank," Knolls Atomic Power Laboratory, KAPL-M-7759 (September 1990).

E.14. J. T. Mihalczo, W. T. King, E. B. Johnson and E.D. Blakeman, " Subcriticality Measurements for a Fuel Solution Tank with Changing Concentration using the Cf-252-Source-Driven Noise Analysis", Meeting of the American Nuclear Society, San Francisco, Trans. Amer. Nucl, Soc. 45, 237-238 (1983)

E.15. E.D. Blakeman and T. E. Valentine, "Unreflected High Enriched Uranyl Nitrate Subcritical Noise measurements" SUB_HEU_SOL_THERM-001, NEA/NSC/DOC/(95)03/II Volume II (2019)

E.16. E. D. Blakeman, Subcritical Noise Measurements for Two Coaxial Cylindrical Tanks Containing 93.1 wt. % Uranyl Nitrate Solution", SUB_HEU_SOL_THERM-002, NEA/NSC/DOC/(95)03/NSC/DOC

APPENDIX F. NEUTRON COUNT RATES-OK

The neutron count rates were measured in all six Oak Ridge National Laboratory neutron detectors and the two Babcock & Wilcox detectors, as shown in Table F.1. The two Babcock & Wilcox detectors were in the water reflector adjacent to the outer core boundary on the N–S core diameter.

Table F.1. Neutron count rates per second for all eight detectors.

Run #	1	2	3	4	5	6	7	8
AE	17,548	17,800	—[a]	—	—	—	—	—
AG	20,000	21,400	—	—	—	—	—	—
AH	—	—	—	—	132,507	142,663	—	—
AI	—	—	122,736	120,353	102,906	103,641	—	—
AL	142,653	69,980	56,205	143,565	70,824	55,892	—	—
AO	23,453	8,913	7,006	23,096	8,907	6,946	—	—
AR	34,056	13,539	10,376	35,135	13,287	10,225	—	—
AU	108,310	77,932	31,518	24,199	112,795	77,063	31,005	—
AY	22,428	15,741	5,577	4,379	23,500	15,579	5,563	4,199
BA	14,491	9,733	3,690	2,851	15,479	19,212	3,594	3,058
BC	43,967	48,271	44,002	42,966	44,215	49,477	42,879	—
BE	4,779	5,227	4,902	1,582	4,778	5,364	4,622	1,510
BF	20,291	21,032	19,751	15,710	20,079	20,651	19,523	15,186
BH	2,251	2,352	2,217	1,817	2,242	2,349	2,339	1,797
BI	64,045	63,113	61,874	11,936	62,342	65,882	63,279	12,104
BL	30,847	30,411	29,981	4,556	29,855	30,728	28,851	4,287
BP	2,717	2,670	2,701	570	2,659	2,730	2,666	521
BQ	16,881	18,965	16,526	4,815	16,535	18t,606	15,685	4,567
BR	16,580	18,482	15,955	4,696	16,177	18,228	15,250	4,618
BW	1,642	1,824	1,614	563	1,607	1,805	1,564	5,994
BX	6,561	6,701	6,337	4,869	6,294	6,447	6,117	4,699
CA	21,914	21,173	21,216	2,828	20,989	21,498	20,383	2,550
CC	21,659	21,371	20,876	2,851	20,756	21,326	20,255	2,535
CE	10,876	12,138	10,489	2,929	10,588	11,892	9,925	2,610
CH	7,192	10,822	14,346	2,646	7,094	10,644	13,455	2,396
CI	4,666	7,992	15,846	2,033	4,597	7,912	14,525	1,839
CJ	49,847	82,122	135,367	22,983	49,819	81,591	126,869	221,180
CK	29,227	52,636	115,084	14,244	29,429	52,818	105,868	13,074
CM	49,255	81,638	134,299	22,723	48,653	80,957	126,393	21,716
CO	10,498	19,912	54,062	5,196	10,456	20,172	50,904	4,889
CP	44,339	45,899	43,037	33,413	43,907	44,637	42,224	3,164
CR	150	183	152	170	140	153	145	150
CU	119,804	122,666	119,243	15,939	116,558	121,530	115,208	14,726
CZ	62,226	69,453	60,600	16,217	60,100	68,255	57,098	15,006
DD	23,157	23,564	21,736	16,144	22,015	22,140	208,217	14,871

Table F.1. Neutron count rates per second for all eight detectors (continued).

Run #	1	2	3	4	5	6	7	8
DG	1,228	1,738	1,283	1,272	1,175	1,626	1,154	1,231
DI	1,159	1,496	788	1,057	1,198	1,447	719	1,019
DJ	129,103	133,303	127,329	176,099	126,025	130,381	121,278	16,246
DL	25,841	27,035	24,541	1,163	25,339	25,778	22,577	1,290
DN	1,688	3,100	1,827	2,179	1,807	2,893	1,833	2,162
DO	2,153	2,482	2,274	2,508	2,142	3,233	1,195	2,582
DP	20,891	22,211	19,274	721	19,635	20,097	17,922	788
DS	8,861	8,835	8,424	730	8,332	8,499	7,712	678
DV	98,188	100,844	95,995	9,459	94,553	98,011	88,937	8,731
DY	88,603	91,048	86,607	8,282	84,981	88,049	80,078	7,601
EB	38,171	42,979	36,554	8,382	36,519	41,810	23,979	7,753
EE	19,824	37,089	60,577	7,363	19,227	36,171	55,178	6,821
EF	10,194	25,243	74,137	5,243	9,876	24,598	65,965	4,856
EG	10,000	24,991	23,793	5,120	9,713	24,188	64,788	4,759
EH	4,726	13,552	61,173	2,931	4,579	13,346	53,862	2,723
EJ	2,255	12,824	2,445	8,383	3,023	11,999	3,201	7,623
EK	12,607	12,767	12,115	8,339	12,006	11,958	11,212	7,733
EM	1,845	1,674	1,836	1,232	1,768	1,529	1,691	1,202
EP	2,023	1,948	1,990	998	1,326	1,326	1,686	952
ES	4,360	3,092	4,124	2,055	2,921	2,921	3,844	1,970
EU	56,253	56,994	53,397	3,250	51,357	53,919	49,684	2,928
EY	18,787	20,852	17,321	3,297	7,491	20,177	15,755	3,022
EZ	18,243	20,939	17,330	3,290	17,514	19,964	15,523	2,922
FB	5,967	5,522	5,778	3,292	5,490	4,986	5,028	2,946
FC	6,663	6,262	6,454	3,758	60,068	5,583	5,785	3,304
FF	14,777	15,814	13,265	308	13,597	14,232	12,345	352
FI	21,155	24,039	19,692	3,711	19,674	22,392	18,083	3,319
FJ	41,670	41,744	38,910	1,615	37,400	38,056	34,975	1,437
FM	11,093	12,961	10,321	1,610	10,163	11,567	9,181	1,406
FO	572	493	558	694	472	438	438	505
FP	3,023	2,823	2,922	1,635	2,661	2,427	2,539	1,657
FT	2,972	2,775	2,872	1,511	2,620	2,372	2,482	—
FV	602	521	584	696	495	442	453	—
FW	114,476	125,883	108,204	—	100,305	114,438	98,735	—
FZ	10,838	11,912	9,844	163	9,822	10,366	8,688	—
GA	8,815	9,550	7,708	106	7,764	8,394	6,933	—
GD	29,521	30,107	17,191	846	25,894	26,398	23,863	—
GG	14,616	13,350	14,333	8,613	13,551	12,048	12,979	—
GH	1,039	948	1,012	731	971	878	955	—
GI	1,006	1,517	3,178	1,045	983	1,395	2,960	—
GJ	74,878	76,194	75,413	3,721	77,130	77,130	73,603	—

Table F.1. Neutron count rates per second for all eight detectors (continued).

Run #	1	2	3	4	5	6	7	8
GN	46,983	53,414	46,978	4,495	45,532	54,913	46,531	—
GR	20,432	20,659	20,904	5,401	21,977	20,735	19,596	—
GV	37,376	37,636	37,108	363	35,186	37,552	--	—
GY	15,825	16,237	15,297	411	15,301	16,025	14,732	—
HB	15,541	16,149	15,179	397	14,920	162,441	14,969	—
HF	13,792	13,368	13,273	90	13,046	13,273	12,666	—
HK	35,491	28,037	33,413	1,539	33,268	35,216	32,247	—
HP	1,223	1,843	1,326	—	1,283	1,518	1,113	—
HQ	1,209	1,858	1,312	—	1,270	1,523	1,130	—
HT	8,275	9,001	7,921	—	7,740	7,468	7,261	—
HY	25,340	27,735	23,522	315	23,400	26,213	22,046	—
IC	19,004	18,244	17,102	1,482	17,384	16,228	15,404	—
II	1,482	1,601	1,363	—	1,377	1,454	1,284	—
IL	14,450	21,819	12,906	1,133	1,454	19,298	11,682	—
IR	1,305	11,102,332	1240	—	1,174	--	1,106	—

[a]Indicates not measured or recorded

APPENDIX G. PARAMETERS FOR INTERPRETATION OF RATIO OF SPECTRAL DENSITIES TO OBTAIN NEUTRON MULTIPLICATION FACTORS FOR ARRAYS OF FRESH PWR FUEL PINS

The parameters in Table G.1 were used to infer the neutron multiplication factors from the ratios of spectral densities for configurations of fresh PWR fuel pins.

Table G.1. Parameters used to obtain the neutron multiplication factors from the ratios of spectral densities.

Number of fuel pins	Boron (ppm)	I_c/I	*R* spatial correction factor	Number of neutrons per fission	β_{eff}	Cf Neutrons per fission	Cf average neutrons per fission squared	Average *ν(ν-1)* over average *ν* times *ν*
4961	1511	3.13	1.2215	2.4255	0.007488	3.773	15.818	0.795
4961	1561	2.567	1.2144	2.4430	0.0074896	3.773	15.818	0.795
4961	1613	2.119	1.2075	2.5248	0.0074904	3.773	15.818	0.795
4961	1765	1.579	1.188	2.4262	0.007474	3.773	15.818	0.795
4961	1880	1.4797	1.4797	2.4265	0.0074958	3.773	15.818	0.795
4961	2104	1.3262	1.1546	2.4457	0.0074982	3.773	15.818	0.795
4961	2386	1.22841	1.136	2.4463	0.0075022	3.773	15.818	0.795
4961	2925	1.0964	1.1195	2.4488	0.0075055	3.773	15.818	0.795
4961	3606	1.04662	1.08105	2.4516	0.0075093	3.773	15.818	0.795
4961	4303	1.02145	1.0525	2.4362	0.007510	3.773	15.818	0.795
3713	1.511	2.42570	1.2064	2.4257	0.007488	3.773	15.818	0.795
2553	1511	2.42570	1.18601	2.4257	0.007595	3.773	15.818	0.795
1281	1511	2.42529	1.20634	2.42529	0.007928	3.773	15.818	0.795
743	1511	2.42552	1.11841	2.42552	0.007988	3.773	15.818	0.795
333	1511	2.42586	1.07772	2.4286	0.008476	3.773	15.818	0.795
269	1511	2.42413	1.0808	2.42413	0.008498	3.773	15.818	0.795